Differential Transmission of Actin Motion Within Focal Adhesions

Ke Hu, *et al.*

Science **315**, 111 (2007);
DOI: 10.1126/science.1135085

Science (print ISSN 0036-8075; online ISSN 1095-9203) is published weekly, except the last week in December, by the American Association for the Advancement of Science, 1200 New York Avenue NW, Washington, DC 20005.

Efficient antigen presentation by DCs requires regulated lysosomal protein degradation (*21*, *22*). However, the requirements for presentation on MHCII and cross-presentation on MHCI differ in that MHCII processing occurs inside endosomes, whereas cross-presentation on MHCI necessitates antigen escape from the endosome into the cytoplasm to gain access to the proteasome and TAP transporters (*19*, *20*, *23*–*25*). Elegant in vitro experiments with cultured DCs show that during DC development, antigen presentation is regulated through control of lysosomal processing and MHCII cell surface transport (*21*, *22*, *26*–*28*). Cultured immature DCs capture antigen but only process and present it on MHCII after exposure to inflammatory stimuli or TLR ligation (*22*). This unique ability to sequester antigens may be important for their preservation during DC transit from sites of inflammation to lymphoid organs and might facilitate the escape of antigen from endosomes to the cytoplasm or endoplasmic reticulum for cross-presentation (*21*). However, DCs that fail to degrade antigen might also be suboptimal producers of MHCII-p. Our experiments show that in the intact host, this problem is resolved by producing a subset of DCs specialized for maximizing MHCII presentation. Although $CD8^{+}DEC205^{+}$ DCs can initiate immune responses by presenting on MHCII, $CD8^{-}33D1^{+}$ DCs excel in producing MHCII-p. This specialization may have important implications for understanding the initiation of T cell responses in vivo and for rational vaccine design.

References and Notes

1. Y. J. Liu, *Cell* **106**, 259 (2001).
2. K. Shortman, Y. J. Liu, *Nat. Rev. Immunol.* **2**, 151 (2002).
3. R. M. Steinman, D. Hawiger, M. C. Nussenzweig, *Annu. Rev. Immunol.* **21**, 685 (2003).
4. D. Vremec *et al.*, *J. Exp. Med.* **176**, 47 (1992).
5. M. D. Witmer, R. M. Steinman, *Am. J. Anat.* **170**, 465 (1984).
6. R. S. Allan *et al.*, *Science* **301**, 1925 (2003).
7. J. M. den Haan, S. M. Lehar, M. J. Bevan, *J. Exp. Med.* **192**, 1685 (2000).
8. T. Iyoda *et al.*, *J. Exp. Med.* **195**, 1289 (2002).
9. J. M. den Haan, M. J. Bevan, *J. Exp. Med.* **196**, 817 (2002).
10. J. L. Pooley, W. R. Heath, K. Shortman, *J. Immunol.* **166**, 5327 (2001).
11. C. Scheinecker, R. McHugh, E. M. Shevach, R. N. Germain, *J. Exp. Med.* **196**, 1079 (2002).
12. P. Schnorrer *et al.*, *Proc. Natl. Acad. Sci. U.S.A.* **103**, 10729 (2006).
13. Materials and methods are available as supporting material on *Science* Online.
14. D. Hawiger *et al.*, *J. Exp. Med.* **194**, 769 (2001).
15. M. C. Nussenzweig, R. M. Steinman, M. D. Witmer, B. Gutchinov, *Proc. Natl. Acad. Sci. U.S.A.* **79**, 161 (1982).
16. L. Bonifaz *et al.*, *J. Exp. Med.* **196**, 1627 (2002).
17. G. Dadaglio, C. A. Nelson, M. B. Deck, S. J. Petzold, E. R. Unanue, *Immunity* **6**, 727 (1997).
18. M. Guo *et al.*, *Hum. Immunol.* **61**, 729 (2000).
19. P. Bryant, H. Ploegh, *Curr. Opin. Immunol.* **16**, 96 (2004).
20. P. Cresswell, N. Bangia, T. Dick, G. Diedrich, *Immunol. Rev.* **172**, 21 (1999).
21. L. Delamarre, M. Pack, H. Chang, I. Mellman, E. S. Trombetta, *Science* **307**, 1630 (2005).
22. E. S. Trombetta, I. Mellman, *Annu. Rev. Immunol.* **23**, 975 (2005).
23. R. N. Germain, *Cell* **76**, 287 (1994).
24. N. Shastri, S. Cardinaud, S. R. Schwab, T. Serwold, J. Kunisawa, *Immunol. Rev.* **207**, 31 (2005).
25. J. W. Yewdell, C. C. Norbury, J. R. Bennink, *Adv. Immunol.* **73**, 1 (1999).
26. K. Inaba *et al.*, *J. Exp. Med.* **191**, 927 (2000).
27. P. Pierre, I. Mellman, *Cell* **93**, 1135 (1998).
28. S. J. Turley *et al.*, *Science* **288**, 522 (2000).

29. We thank K. Velinzon for cell sorting; K.-H. Yao for technical assistance; H.-K. Lee, S. H. Park, and S. Y. Joe for help generating CD11c-hDEC205 mice; A. Flores-Langarica, S. Boscardin, A. Gazumyan, E. Besmer, and F. Nimmerjahn for helpful discussion; the MSKCC Monoclonal Antibody Core Facility for labeling of antibodies; and MSKCC Genomics Core Laboratory for performing the microarrays. Supported by grants from the NIH (to C.G.P., R.M.S., and M.C.N.). D.D. is a fellow of the Deutsche Forschungsgemeinschaft (DU 548/1-1), and V.R.B. was supported by the German National Academic Foundation. M.C.N. is an Investigator with the Howard Hughes Medical Institute. M.C.N. and R.M.S. are on the scientific advisory board of Celldex, a startup company interested in targeting dendritic cells.

Supporting Online Material

www.sciencemag.org/cgi/content/full/315/5808/107/DC1
Materials and Methods
Figs. S1 to S11
References

10 October 2006; accepted 15 November 2006
10.1126/science.1136080

Differential Transmission of Actin Motion Within Focal Adhesions

Ke Hu,* Lin Ji,* Kathryn T. Applegate, Gaudenz Danuser,† Clare M. Waterman-Storer†

Cell migration requires the transmission of motion generated in the actin cytoskeleton to the extracellular environment through a complex assembly of proteins in focal adhesions. We developed correlational fluorescent speckle microscopy to measure the coupling of focal-adhesion proteins to actin filaments. Different classes of focal-adhesion structural and regulatory molecules exhibited varying degrees of correlated motions with actin filaments, indicating hierarchical transmission of actin motion through focal adhesions. Interactions between vinculin, talin, and actin filaments appear to constitute a slippage interface between the cytoskeleton and integrins, generating a molecular clutch that is regulated during the morphodynamic transitions of cell migration.

Directed cell migration involves spatiotemporal orchestration of protrusion at the leading cell edge, adhesion of the protrusion to the extracellular matrix (ECM), pulling against the adhesions to translocate the cell body, and weakening of the adhesion at the cell rear for advancement (*1*). In this process, actin filaments (F-actin) must couple to the ECM through the plasma membrane (*1*–*3*) via focal adhesions (FAs) to translate actin polymerization and/or actin-myosin contraction into cell motion. FAs are complexes of >100 different proteins linking F-actin to clustered transmembrane integrin ECM receptors (*2*, *4*). Regulating the attachment between F-actin and integrins via proteins within FAs is thought to be critical for controlling the spatiotemporal variability of protrusion and traction (*5*) and the ability of cells to respond to mechanical cues.

It is well established that F-actin and FAs are coupled to each other. Many FA proteins bind directly or indirectly to F-actin (*6*–*8*) and/or integrins (*9*–*13*). Contractile actomyosin bundles are often rooted in FAs (*2*, *4*), and perturbations of actomyosin cause changes in FAs and vice versa (*2*). Although the importance of spatiotemporal coordination between FAs and F-actin in cell migration is well appreciated (*2*, *14*, *15*), it is not known which FA molecules interact with F-actin in living cells, and the dynamics of molecules within these two assemblies have never been analyzed simultaneously. Predicting how FA proteins behave in vivo by biochemical data alone is impossible because of the complexity of their interactions (*4*).

To study the dynamic interactions between F-actin and FAs, we combined total internal reflection fluorescence microscopy (TIRFM) and fluorescent speckle microscopy (FSM). TIRFM optimizes image contrast at the ventral cell–ECM/coverslip interface where cortical F-actin integrates with FAs. FSM marks macromolecular assemblies with fluorophore clusters called speckles (fig. S1). Computational tracking of speckle motion allows mapping of protein dynamics with submicron resolution (*16*, *17*). We studied PtK1 cells migrating on coverslips, on which they organized a fibronectin-containing ECM (fig. S2).

To determine the spatial relations between FAs and F-actin flow, we captured image pairs using TIRFM of green fluorescent protein

Department of Cell Biology, The Scripps Research Institute, La Jolla, CA 92037, USA.

*These authors contributed equally to this work.
†To whom correspondence should be addressed. E-mail: waterman@scripps.edu (C.M.W.-S.); gdanuser@scripps.edu (G.D.)

(GFP)–vinculin and TIR-FSM of X-rhodamine actin (Fig. 1). As seen previously (*16*), the narrow meshwork of F-actin in the lamellipodium underwent rapid retrograde flow from the leading edge toward the cell center. Proximal to this, F-actin retrograde flow in the lamella was slower. An overlay of FAs onto the F-actin flow map revealed that the negative flow speed gradient at the lamellipodium/lamella junction corresponded to the distal boundaries of FAs (Fig. 1, C and D). Thus, FAs may locally dampen flow by engaging F-actin to the ECM. The global slowing of F-actin flow in the lamella is probably due to the uniform distribution of FAs and the small inter-FA spacing in this cell region. Despite the slowing, F-actin retrograde flow within FAs was substantial and coherent (Fig. 1C) (*18*). Thus, if an interaction between FA proteins and F-actin occurs in living cells, movement of proteins within FAs is likely.

To analyze the motion of proteins within FAs, we performed TIR-FSM on cells expressing three classes of GFP-conjugated FA proteins: first, a fibronectin-binding integrin (GFP–α_v integrin coexpressed with untagged β_3 integrin); second, FA proteins capable of binding directly to F-actin [α-actinin (*6*), vinculin (*8*, *19*), and talin (*6*, *20*)]; and third, FA "core" proteins that do not bind F-actin or the ECM directly but include structural and signaling molecules [paxillin (*9*, *21*), zyxin (*12*), and focal-adhesion kinase (FAK) (*13*)]. We focused on FAs in the ~100-nm-thick leading-edge lamella, where F-actin forms transverse bundles, isotropic networks, and stress fibers (*22*), all of which are within the evanescent excitation field. FA speckles were tracked within segmented FA regions, and average speckle speeds and coherencies were computed (*18*). Monte Carlo simulations showed that random binding and dissociation of fluorescent molecules to and from an immobile FA produced speckle velocities <0.05 μm/min and coherencies <0.4 on a scale of 0 to 1 (fig. S7), similar to measurements of X-rhodamine–actin speckles imaged in a fixed cell (*18*) and thus defining the detection limit of our measurements.

We found highly diverse behaviors of the seven GFP–FA proteins within FAs (Fig. 2 and tables S1 and S2). Speckles consisting of FA proteins with no known F-actin–binding activity moved slowly and mostly incoherently (Fig. 2, movies S1 to S3, and tables S1 and S2). Of these, GFP–$\alpha_v\beta_3$ integrin was the slowest and the most incoherent (Fig. 2C and movie S1), probably due to its immobilization by binding to the ECM on the coverslip. FA core proteins were slightly more motile than $\alpha_v\beta_3$ integrin, with a retrograde directional bias in their movement (Fig. 2, D to F). GFP-zyxin and GFP-paxillin moved somewhat more coherently than GFP–$\alpha_v\beta_3$ integrin, whereas GFP-FAK speckles moved faster than GFP–$\alpha_v\beta_3$ integrin (Fig. 2, D to F; movie S2; and tables S1 and S2).

In contrast, all three GFP-tagged FA actin–binding proteins moved coherently within the FAs. The dynamics of FA actin–binding proteins were significantly different from those of both the

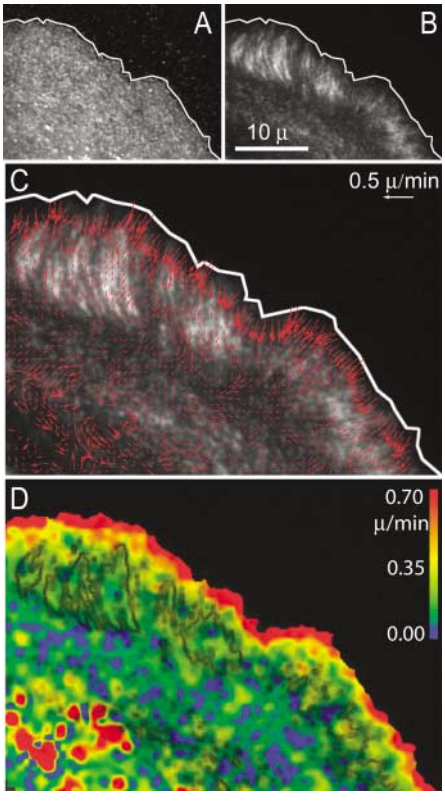

Fig. 1. F-actin motion relative to FAs at the leading edge of a migrating PtK1 epithelial cell. (**A**) TIR-FSM image of X-rhodamine actin and (**B**) TIRF image of GFP-vinculin. (**C**) Velocity vectors of F-actin speckle motion averaged over 100 s are overlaid on the TIRF image of GFP-vinculin. (**D**) Color-coded map of F-actin speed, with FAs outlined in gray.

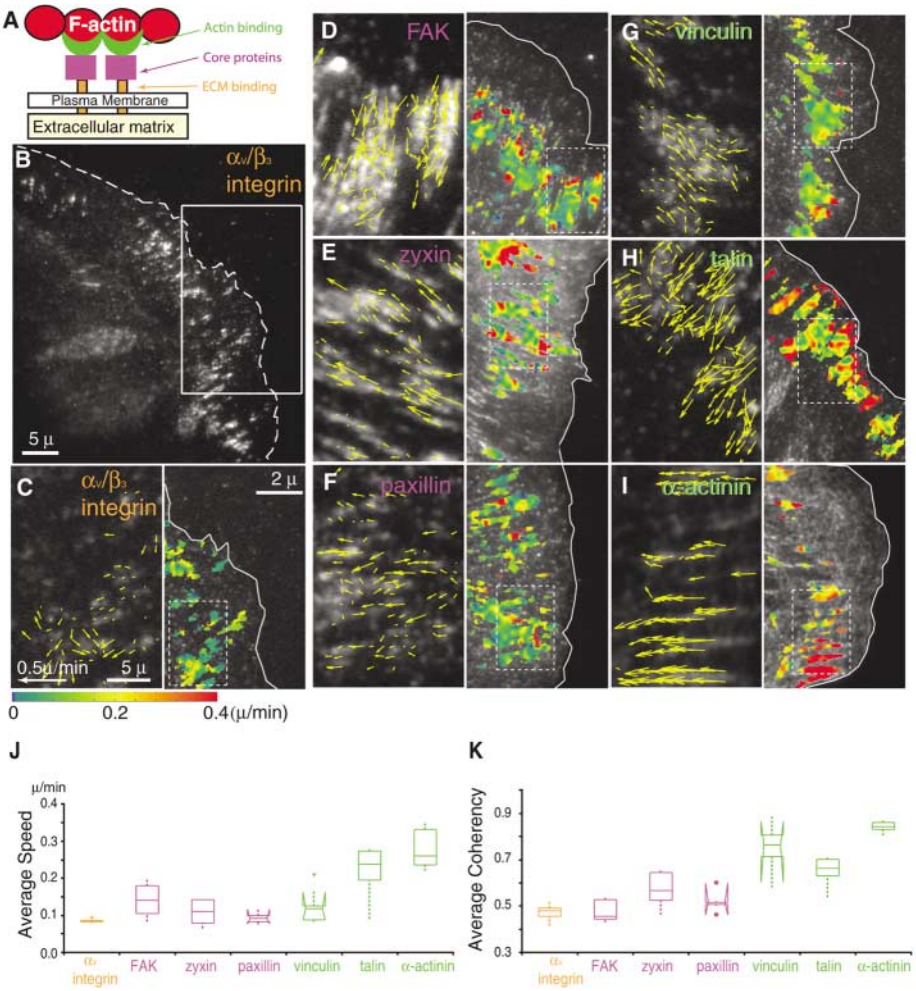

Fig. 2. The motions of different proteins within FAs are diverse. (**A**) Classes of FA molecules analyzed. FA-actin–binding proteins, green; FA core proteins, purple; integrins, orange. (**B**) TIR-FSM image of a cell coexpressing GFP–α_v integrin and untagged β_3 integrin. White frame, region shown in (C), on the right. (**C** to **I**) Velocity vectors (left) and speed maps (right, boxed area shown at left) of seven GFP-tagged FA proteins analyzed by TIR-FSM. (**J** and **K**) Average speed and velocity coherency of FA molecules [also see tables S1 and S2 (*18*) and fig. S3A].

integrin and core proteins and also from each other (Fig. 2, G to I; movie S3; and tables S1 and S2). GFP–α-actinin speckles moved fastest and most coherently. GFP-vinculin speckles moved slowly but highly coherently, whereas GFP-talin speckle motion was the least coherent of all three, but it was significantly faster than vinculin. Speed maps revealed that speckle speeds could vary within individual FAs and between adjacent FAs (Fig. 2, C to I). None of these FA proteins possess motor activity or interact with motor proteins, which suggests that their motion is influenced by interactions with other dynamic cell components, such as F-actin.

To determine whether the motion of proteins within FAs was related to F-actin flow, we developed correlational FSM to quantify the degree of motion correlation between GFP-FA and X-rhodamine–F-actin speckles (*18*). As verified by Monte Carlo simulations, a high degree of speckle motion correlation indicates concerted movement of molecules as part of the same macromolecular ensemble, mediated by direct or indirect interactions. We tracked speckle motion within FAs in both channels and interpolated speckle velocities onto a common 0.45-μm–by–0.45-μm grid to allow comparison of pairs of FA and F-actin flow vectors (fig. S3).

To determine the dependency between the velocities of FA protein and F-actin speckles, we performed linear regression of scatter plots of FA versus F-actin speckle velocities averaged within individual FAs (Fig. 3A and fig. S5A). This revealed velocity correlations between F-actin and the FA actin–binding proteins vinculin, α-actinin, and talin. The relatively low correlation coefficient for talin indicated a high variability in the talin–F-actin interaction.

To estimate the extent of molecular coupling between F-actin and FA molecules, we computed two parameters: direction coupling score (DCS = cos θ, where θ is the angle between paired FA and F-actin vectors), to measure the directional similarities between FA and F-actin speckle motions, and velocity magnitude coupling score (VMCS) (Fig. 3B and fig. S3), to measure relative FA speckle motion along the local F-actin flow axis, thus accounting for both direction and speed. For identical speckle flow fields, both DCS and VMCS are equal to 1 (see Fig. 3, G to H; tables S3 to S5; and fig. S4 for analysis of GFP- and Alexa 568–actin in the same cell).

Analysis of FAs in the lamella revealed that couplings between different FA molecules and F-actin were highly diverse (tables S4 and S5). FA core proteins and $\alpha_v\beta_3$ integrin both exhibited a DCS and a VMCS much less than 1 (Fig. 3, fig. S5, movies S5 to S8, and tables S4 and S5). Therefore, a substantial portion of the motion of

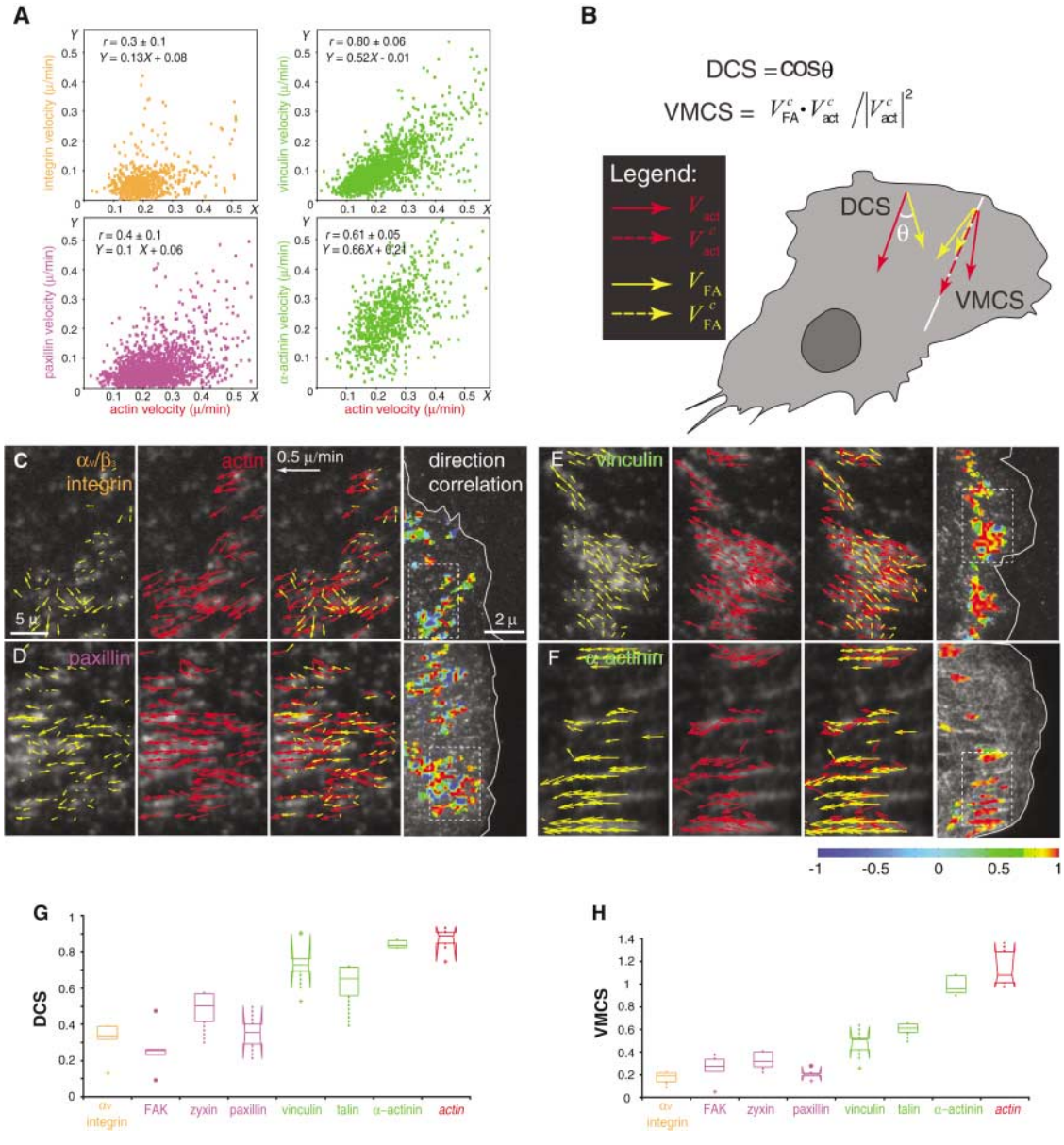

Fig. 3. Correlational FSM reveals that proteins within FAs are differentially coupled to F-actin motion. (**A**) FA versus F-actin speckle motions. Each point represents the average FA and F-actin speckle velocities within one FA at one time step. Correlation coefficients (*r*) and two times the standard deviation are indicated (bootstrap regression, 200 trials). *Y*, FA protein velocity; *X*, F-actin velocity. (**B**) Definitions of DCS and VMCS [also see (*18*) and fig. S3]. V_{FA} and V_{act} are the actual velocity measurements, and V^c_{FA} and V^c_{act} are the coupled components of the flow vectors. (**C** to **F**) Correlational FSM analysis of GFP–$\alpha_v\beta_3$ integrin (C), paxillin-GFP (D), vinculin-GFP (E), and α-actinin–GFP (F). From left to right in each panel are FA speckle velocity, F-actin speckle velocity, an overlay of the two velocities, and a color-coded DCS map. (**G** and **H**) Average DCS (G) and VMCS (H) between FA molecules and F-actin (averages from several cells, tables S4 and S5). Red, scores for a cell containing GFP-actin and Alexa 568–actin (fig. S4).

FA core proteins and $\alpha_v\beta_3$ integrin was not related to F-actin flow but was probably caused by interactions with other binding partners within FAs that immobilize them or deviate their motion from the F-actin flow axis. Alternatively, binding and dissociation of FA proteins to and from FAs could also generate random minor speckle displacements (figs. S6 and S7).

The motions of FA actin–binding proteins within FAs all showed significantly greater coupling to F-actin motion than did core proteins and $\alpha_v\beta_3$ integrin, although they were clearly different from each other (movies S9 to S11 and tables S4 and S5). α-Actinin displayed the highest coupling to F-actin motion (movie S11). This is expected because α-actinin mimics the kinematics of F-actin throughout the cell, indicating its tight association with F-actin, irrespective of localization (*23*, *24*). Both vinculin and talin were significantly, yet partially, coupled to F-actin motion, indicating partial transmission of F-actin motion to these proteins within FAs (tables S4 and S5).

Mapping local DCS revealed heterogeneity in coupling between F-actin and FA proteins within individual FAs and between adjacent FAs (Fig. 3, C to F). To see whether this heterogeneity was related to whole-FA dynamics or cell migration behavior, we performed correlational FSM for vinculin and F-actin (Fig. 4A and movie S12) at the leading edge of a cell where one area protruded and an adjacent area retracted (Fig. 4A). The protrusive area contained a FA that remained stationary, whereas the FA in the retracting area slid rearward and later stabilized (Fig. 4A). In the stationary FA, the speeds of F-actin and vinculin speckle flow and the DCS and VMCS between F-actin and vinculin remained relatively constant, with only small fluctuations over time (Fig. 4B). In contrast, in the sliding FA, the speeds of actin and vinculin and their VMCS and DCS increased before FA sliding (Fig. 4C). The coupling between vinculin and F-actin peaked during FA sliding and decreased before FA stabilization. Thus, dissociation of vinculin from a less mobile FA component and stable vinculin–F-actin binding may initiate FA disengagement from the ECM, whereas partial coupling between vinculin and F-actin may be necessary for establishing and/or maintaining the engagement between the FA and the ECM.

Our direct analysis of the dynamic interactions between FA components and F-actin in living cells reveals that the efficiency of motion transmission from F-actin to FA proteins within FAs decreased from actin-binding proteins to FA core proteins to integrin, defining a hierarchical slippage clutch. This is likely to be the result of differential transmission of F-actin–based force through a network of transient protein-protein interactions in FAs. Partial coupling of talin and vinculin to F-actin motion could represent these molecules spending part of

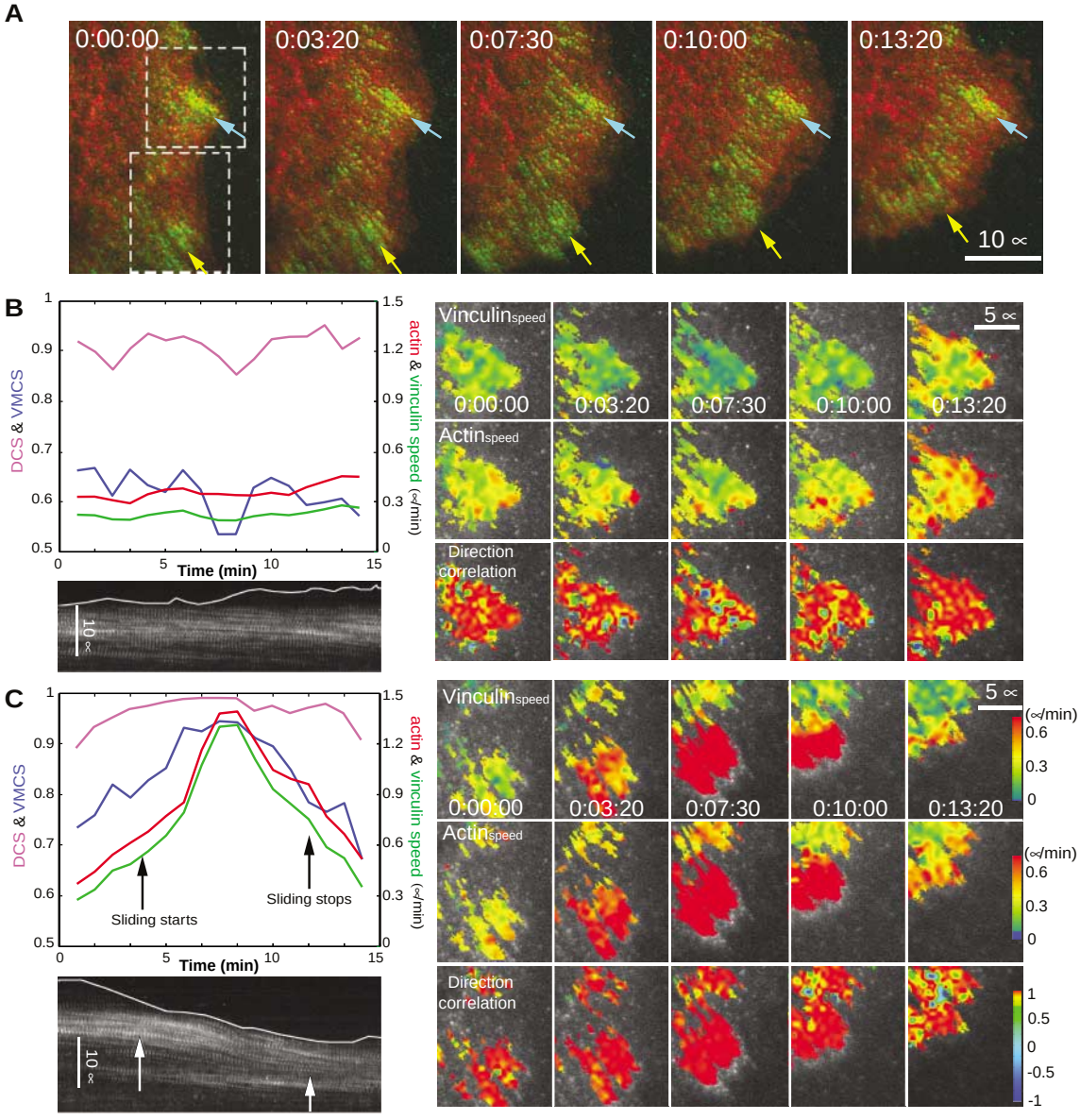

Fig. 4. Vinculin–F-actin coupling is time-modulated during the retraction of a FA. (**A**) Images of GFP-vinculin (green) and X-rhodamine–actin (red). Blue arrow, stable FA in a protrusive cell region; yellow arrow, sliding FA in a retracting cell region; white frames, regions of interest analyzed by FSM in (B) and (C). (**B** and **C**) Temporal variation of F-actin and vinculin speckle speeds, DCS, and VMCS within a stable (B) and a sliding (C) FA. Top left panels show graphs of average speeds of F-actin (red) and vinculin (green) speckles, vinculin-actin VMCS (blue), and vinculin-actin DCS (pink). Bottom left panels show kymographs of GFP-vinculin taken along the axes of arrows in (A). The position of the cell edge in white shows that the FA remains stationary in (B), whereas in (C) the FA initiates sliding at ~4 min (left arrow) and stops at ~12 min (right arrow). Right panels show maps of vinculin and actin speckle speeds and DCS. During retraction and FA sliding, vinculin alters its binding to F-actin. Time is given in hour:min:sec.

their time bound to moving F-actin and part of their time bound to a less mobile FA component, thus identifying these proteins as a site of slippage in the F-actin/FA interface. Alternatively, differential coupling of FA proteins to transverse actin bundles and stress fibers in the lamella could contribute to the observed effect. However, given the local slowing of F-actin flow in the FA in the lamella and the biophysical evidence implicating talin and vinculin in force transmission in the FA (*20*, *25*, *26*), we suspect that these proteins form transient linkages across the slippage interface, resulting in force-transducing slip-stick friction between F-actin and the ECM. The degree of molecular motion transmission through the FA was regulated, and it was correlated with protrusion and retraction events during cell migration. Therefore, FA internal molecular kinematics may be a key element in the integrin-mediated translation of intracellular biochemistry into cellular mechanics during cell and tissue morphogenesis, or in the reception of extracellular mechanical signals to mediate sensory perception, tissue maintenance, and differentiation (*27*).

References and Notes

1. D. A. Lauffenburger, A. F. Horwitz, *Cell* **84**, 359 (1996).
2. K. Burridge, M. Chrzanowska-Wodnicka, *Annu. Rev. Cell Dev. Biol.* **12**, 463 (1996).
3. C. H. Lin, P. Forscher, *Neuron* **14**, 763 (1995).
4. B. Geiger, A. Bershadsky, R. Pankov, K. M. Yamada, *Nat. Rev. Mol. Cell Biol.* **2**, 793 (2001).
5. R. J. Pelham Jr., Y. Wang, *Proc. Natl. Acad. Sci. U.S.A.* **94**, 13661 (1997).
6. K. Maruyama, S. Ebashi, *J. Biochem. (Tokyo)* **58**, 13 (1965).
7. M. Muguruma, S. Matsumura, T. Fukazawa, *Biochem. Biophys. Res. Commun.* **171**, 1217 (1990).
8. R. P. Johnson, S. W. Craig, *Nature* **373**, 261 (1995).
9. T. Tanaka, R. Yamaguchi, H. Sabe, K. Sekiguchi, J. M. Healy, *FEBS Lett.* **399**, 53 (1996).
10. D. A. Calderwood *et al.*, *J. Biol. Chem.* **274**, 28071 (1999).
11. K. Burridge, P. Mangeat, *Nature* **308**, 744 (1984).
12. M. C. Beckerle, *Bioessays* **19**, 949 (1997).
13. D. D. Schlaepfer, T. Hunter, *Cell Struct. Funct.* **21**, 445 (1996).
14. K. M. Yamada, S. Miyamoto, *Curr. Opin. Cell Biol.* **7**, 681 (1995).
15. M. Chrzanowska-Wodnicka, K. Burridge, *J. Cell Biol.* **133**, 1403 (1996).
16. A. Ponti, M. Machacek, S. L. Gupton, C. M. Waterman-Storer, G. Danuser, *Science* **305**, 1782 (2004).
17. L. Ji, G. Danuser, *J. Microsc.* **220**, 150 (2005).
18. Materials and methods are available as supporting material on *Science* Online.
19. B. Geiger, *Cell* **18**, 193 (1979).
20. G. Jiang, G. Giannone, D. R. Critchley, E. Fukumoto, M. P. Sheetz, *Nature* **424**, 334 (2003).
21. C. E. Turner, J. R. Glenney Jr., K. Burridge, *J. Cell Biol.* **111**, 1059 (1990).
22. S. L. Gupton *et al.*, *J. Cell Biol.* **168**, 619 (2005).
23. M. Edlund, M. A. Lotano, C. A. Otey, *Cell Motil. Cytoskelet.* **48**, 190 (2001).
24. G. Giannone *et al.*, *Cell* **116**, 431 (2004).
25. R. M. Ezzell, W. H. Goldmann, N. Wang, N. Parasharama, D. E. Ingber, *Exp. Cell Res.* **231**, 14 (1997).
26. G. Giannone, G. Jiang, D. H. Sutton, D. R. Critchley, M. P. Sheetz, *J. Cell Biol.* **163**, 409 (2003).
27. A. Katsumi, A. W. Orr, E. Tzima, M. A. Schwartz, *J. Biol. Chem.* **279**, 12001 (2004).

28. We thank C. Otey (University of North Carolina, Chapel Hill), A. Huttenlocher (University of Wisconsin, Madison), D. Schlaepfer (Scripps), A. F. Horwitz (University of Virginia, Charlottesville), I. Kaverina (Vanderbilt University), and M. Ginsberg (University of California, San Diego) for complementary DNAs. Supported by NIH grants GM67230 (C.M.W.-S. and G.D.) and U54GM64346 (G.D. and L.J.), American Heart Association Established Investigatorship and NIH Director's Pioneer Award (C.M.W.-S.), Leukemia and Lymphoma Society (K.H.), and NSF (K.T.A.).

Supporting Online Material

www.sciencemag.org/cgi/content/full/315/5808/111/DC1
Materials and Methods
Figs. S1 to S8
Tables S1 to S5
References
Movies S1 to S14

13 September 2006; accepted 16 November 2006
10.1126/science.1135085

Live-Cell Imaging of Enzyme-Substrate Interaction Reveals Spatial Regulation of PTP1B

Ivan A. Yudushkin,[1]* Andreas Schleifenbaum,[1]* Ali Kinkhabwala,[1]* Benjamin G. Neel,[2] Carsten Schultz,[1] Philippe I. H. Bastiaens[1]†

Endoplasmic reticulum–localized protein-tyrosine phosphatase PTP1B terminates growth factor signal transduction by dephosphorylation of receptor tyrosine kinases (RTKs). But how PTP1B allows for RTK signaling in the cytoplasm is unclear. In order to test whether PTP1B activity is spatially regulated, we developed a method based on Förster resonant energy transfer for imaging enzyme-substrate (ES) intermediates in live cells. We observed the establishment of a steady-state ES gradient across the cell. This gradient exhibited robustness to cell-to-cell variability, growth factor activation, and RTK localization, which demonstrated spatial regulation of PTP1B activity. Such regulation may be important for generating distinct cellular environments that permit RTK signal transduction and that mediate its eventual termination.

Protein-tyrosine phosphorylation is widely used by eukaryotic cells to transduce signals, but the dynamic interplay between receptor tyrosine kinases (RTKs) and protein-tyrosine phosphatases (PTPs) remains poorly understood (*1*, *2*). The protein tyrosine phosphatase–1B (PTP1B) resides on the surface of the endoplasmic reticulum (ER) (*3*, *4*) and helps terminate signaling by multiple RTKs, including the epidermal growth factor receptor (EGFR) (*5*). Previous reports demonstrate that RTK signaling occurs at the plasma membrane and endosomes (*6*), and its termination occurs along the ER surface (*7*–*11*). Because PTP1B has much higher specific activity than typical RTKs in vitro (*12*, *13*), uniformly high PTP1B activity along the ER could prevent endosomal RTK signaling. To account for compartmentalized RTK signaling, we hypothesized that PTP1B might exist inside cells as spatially separated subpopulations with different kinetic properties.

To test this hypothesis, we developed an imaging approach based on Förster resonant energy transfer (FRET) to spatially resolve enzyme-substrate (ES) interactions and thereby to monitor enzyme activity in live cells (Fig. 1A) (*11*). We tagged PTP1B with a donor chromophore by fusion to a genetically encoded fluorescent protein, and conjugated the substrate, a synthetic phosphotyrosine-containing peptide, to an acceptor chromophore (Fig. 1B). For Michaelis-Menten kinetics, the steady-state fraction (α) of ES complex to total enzyme (E_0) is as follows:

$$\alpha = ES/E_0 = S/(K_M + S) \qquad (1)$$

where S is the substrate concentration, and K_M is the Michaelis-Menten constant. The fraction α can be mapped across the cell by quantitatively imaging FRET with the use of fluorescence lifetime imaging microscopy (FLIM) (*14*–*16*).

We first tested whether formation of the ES intermediate could be detected by FRET in vitro. To stabilize the ordinarily transient ES intermediate and thereby to facilitate FRET detection, we used the purified enhanced green fluorescent protein (EGFP)–tagged catalytically impaired mutant of PTP1B that retains substrate-binding ability (residues 1 to 321, $PTP1B^{D181A}$, in which Ala^{181} was substituted for Asp) (*17*, *18*). Indeed, FRET in the ES complex was apparent, as in-

[1]European Molecular Biology Laboratory (EMBL), Meyerhofstrasse 1, D-69117 Heidelberg, Germany. [2]Cancer Biology Program, Division of Hematology-Oncology, Department of Medicine, Beth Israel Deaconess Medical Center, Harvard Medical School, 77 Avenue Louis Pasteur, Boston, MA 02115, USA.

*These authors contributed equally to this work.
†To whom correspondence should be addressed. E-mail: bastiaen@embl.de

Supporting Online Material for

Differential Transmission of Actin Motion Within Focal Adhesions

Ke Hu, Lin Ji, Kathryn T. Applegate, Gaudenz Danuser,* Clare M. Waterman-Storer*

*To whom correspondence should be addressed. E-mail: waterman@scripps.edu (C.M.W.-S.); gdanuser@scripps.edu (G.D.)

Published 5 January 2007, *Science* **315**, 111 (2007)

DOI: 10.1126/science.1135085

This PDF file includes:

Other Supporting Online Material for this manuscript includes the following: (available at www.sciencemag.org/cgi/content/full/315/5808/111/DC1)

Supporting On-line Material

Materials and Methods

Cell culture and microinjection:

Ptk1 cells were cultured in media containing 10% fetal bovine serum on # 1.5 glass coverslips for 24-48 hours before microinjection as described previously (*S1*). For simultaneous analysis of F-actin and focal adhesion (FA) proteins, 100μg/ml plasmid DNA encoding eGFP-conjugated FA protein was mixed with 1-2 mg/ml x-rhodamine-actin prepared as described previously (*S2*) or Alexa-568 -conjugated actin (A12374, Molecular Probes) and microinjected into the cell nucleus using an Eppendorf Transjector 5246 (Eppendorf Inc.). Time-lapse imaging was performed 4-6 hours after microinjection, with the exception of the GFP-talin/x-rhodamine-actin movies, where imaging was performed ~12 hours after microinjection due to inefficient expression from the PEGFP-talin plasmid. For integrins, 100μg/ml each of a plasmid expressing human α_V-integrin tagged with GFP and of a plasmid expressing untagged β_3-integrin (see below) were co-injected to ensure proper pairing between alpha and beta subunits of the integrins.

DNA Constructs:

P*h*α_V –integrin-EGFP was constructed as follows:

Vector backbone (Phk012):

A vector (Phk012) containing a GSGPGTGP linker in front of EGFP was first constructed as follows:

EGFP coding sequence was amplified from vector PEGFP-N1 (Clontech) by PCR using Pfu Ultra (Stratagene) using primers:

Sense:

5'ATGCggatccGGTCCTGGAACTGGTCCGGTGAGCAAGGGCGAGGAGCTGTTCACC-3'

Antisense:

5'- GATCTAGAGTCgcggccgcTTTACTTG- 3'

The PCR product was digested with BamHI and NotI, and then ligated in place of EGFP in PEGFP-N1 to result in the plasmid Phk009 that contained a GSGPGTGP linker in front of the EGFP coding sequence.

Phk009 was then digested by NheI and SalI, blunt ended by 3' filling-in using Klenow fragment (NEB, M0210), and religated to destroy the enzyme sites between NheI and SalI, to result in the plasmid Phk012.

Amplification of α_V-integrin coding sequence:

The human α_V -integrin coding sequence was amplified from the vector α_V –integrin PCDNA3.1 (a kind gift from Dr. Mark Ginsberg, UCSD, School of Medicine) by PCR using Pfu ultra (Stratagene) with primers:

Sense: 5'— ACTGggtaccTCGGCGATGGCTTTTCCGCCGCGGCGACGGCTGC—3'

Antisense: 5'—AGCTggatccCGGAGTTTCTGAGTTTCCTTCACCATTTTC—3'

The PCR product was digested with KpnI and BamHI and ligated into Phk012 similarly digested, and the resulting plasmid Phk022 contained EGFP separated from α_V -integrin by a linker of PGSGPGTGP.

The plasmid expressing untagged human β_3-integrin, phk023, was constructed as follows:

Vector backbone (Phk010):

The EGFP coding sequence was amplified from vector PEGFP-N1 (Clontech, GenBank Accession # U55762) by PCR using Pfu Ultra (Stratagene) using primers:

Sense: 5'—ATGCggatccGGTCCTGGAACTGGTCCGGTGAGCAAGGGCGAGGAGCTGTTCACC—3'

Antisense:

5'—ACTGgcggccgcTACCGGTTTACTTGTACAGCTCGTCCATGCCGAG—3'

The PCR product was digested with BamHI and NotI, and then ligated in place of EGFP in PEGFP-N1 and resulted in plasmid Phk010.

Amplification of β_3-integrin coding sequence:

β_3-integrin coding sequence was amplified from vector BS3a (*S3*)(a kind gift from Dr. Mark Ginsberg, UCSD, School of medicine) by PCR using Pfu ultra (Stratagene) with primers:

Sense: 5'—AGTCgctagcGCGGACGAGATGCGAGCGCGGCCGCGG—3'

Antisense: 5'—ATGCaccggtTCATTAAGTGCCCCGGTACGTGATATTGG—3'

The PCR product was digested with NheI and AgeI and ligated into Phk010 similarly digested, resulting in Phk023, the plasmid expressing un-tagged human β_3-integrin.

PEGFP-vinculin was constructed as described in (*S4*). Plasmids expressing other GFP tagged FA molecules were kind gifts from various labs, including Dr. Carol Otey (University of North Carolina, Chapel Hill): PEGFP-α-actinin (*S5*); Dr. Anna Huttenlocher (University of Wisconsin, Madison): PEGFP-talin (*S6*); Dr. David Schlaepfer (Scripps Research Institute): PEGFP-FAK; Dr. Rick Horwitz (University of Virginia): PEGFP-paxillin (*S7*), Dr. Irina Kaverina (Vanderbilt University): PEGFP-zyxin (*S8*).

Immunofluorescence:

For visualizing fibronectin and F-actin, Ptk1 cells plated on glass coverslips for 2 days were fixed with 4% paraformaldehyde for 15min, permealized with 1% TritonX-100 for 15min, treated with 50mM glycine for 15 min to quench free aldehyde groups, blocked with 1% BSA for 1 hour; incubated with rabbit anti-fibronectin (1:200 dilution, F-3648, Sigma-Aldrich) for 1 hour; followed by 1hr-incubation in Cy2-conjugated goat anti-rabbit (1:200 dilution, 111-225-144, Jackson ImmunoResearch) mixed with Alexa-568-Phalloidin (3unit/ml, A-12380, Molecular Probes). Antibodies were diluted in blocking buffer (1% BSA in PHEM buffer (60mM KPipe PH6.9, 25mM Hepes PH7.2, 10mMEGTA, 2mMMgCl_2)). All fixing, permeablization, quenching, blocking and washing solutions were made in PHEM buffer. All reactions were carried out at room temperature.

Live cell imaging:

Cells were maintained at 37^{o}C (Bionomic controller, BC-100, 20/20 Technologies Inc.) on the microscope in culture medium containing 30µl/ml of oxyrase (Oxyrase, Inc.) to inhibit photo-toxicity and photobleaching of x-rhodamine or Alexa568. Injected cells expressing low levels of GFP-FA proteins were chosen for imaging. Pairs of x-rhodamine and GFP TIR-FSM images were acquired at 10 sec intervals over time using a 100x 1.45 NA TIRF objective (Nikon) on a Nikon TE2000U microscope custom-modified with a TIRF (*S9*) illumination module as described in (*S4*). 488nm or 568 nm laser lines from a 50mW KrAr laser (Melles Griot) were selected with a polychromatic acousto-optical modulator (Neos). A dual wavelength dichromatic mirror introduced illumination to the specimen (Chroma). Laser illumination was adjusted to impinge on the coverslip at an angle to yield a calculated evanescent field depth of 120-150nm. An electronic filterwheel with bandpass filters for GFP and x-rhodamine fluorescence selected emission. Images were acquired on a 14 Bit cooled CCD camera (ORCA-ERII; Hamamatsu) controlled through Metamorph software (Molecular Devices Inc.).

Image analysis:

In the following section, we describe the tracking of FA and F-actin speckle motion in TIR-FSM image series, the interpolation of the two resulting speckle flow fields onto common grid points for correlative analysis, the identification of FA sites, the correlation of FA and F-actin speckle flow fields within FA sites, as well as the coherency test and the threshold setting for noise control in our analysis (Fig S3).

Speckle tracking and interpolation of vector fields

x-rhodamine F-actin speckles and GFP-FA protein speckles were tracked separately in image series of each channel using time-integrated cross-correlation tracking (*S10*). The method accumulates evidence from multiple frames to estimate, by cross-correlation, the average motion of the speckle signals in a template over a time window. As discussed in (*S10*), with this approach high tracking accuracy and stability can be achieved despite the weak and noisy speckle signal. For all experiments, the time window for evidence accumulation was set to 10 frames. To increase sampling, consecutive accumulation windows were overlapped by 5 frames resulting in a flow estimate in time points separated by 5 frames (Fig S3A). Therefore, changes in the flow were detectable at a time scale of 50 sec (5 frames x 10 sec interval). Template sizes were adaptively chosen between 11x11 and 21x21 pixels (1 pixel = 0.064μm) depending on the local speckle image contrast (*S10*). This corresponds to 1.5 – 3 times the diameter of a speckle. Templates were placed on the positions of significant F-actin and GFP-FA protein speckles (*S11*) and on a 10x10 pixel grid to ensure that all speckles are tracked explicitly where detectable, while covering the whole field of view.

The origins of FA protein and F-actin speckle flow vectors were generally not co-localized, due to the random nature of speckle positions. To allow direct comparison of FA protein and F-actin flow, the tracked flow vectors from both channels were interpolated to common grid points at 7x7 pixel spacing, matching the speckle density (Fig S3B). The interpolation relied on a distance-weighted average based on a Gaussian kernel centered on each grid point:

$$V_{\text{grid}}(x_{\text{grid}}, y_{\text{grid}}) = \frac{1}{W} \sum_{i}^{d_i \le 2\sigma} w_i V_i(x_i, y_i), w_i = e^{-d_i^2/(2\sigma^2)}, d_i = \sqrt{(x_i - x_{\text{grid}})^2 + (y_i - y_{\text{grid}})^2}\ .$$

In this formula, V_{grid} is the interpolated flow velocity, V_i represents the tracked flow and $W = \sum_{i}^{d_i \le 2\sigma} w_i$ is the total weight. In agreement with the speckle density, we chose σ for the Gaussian kernel = 5 pixels.

Segmentation of Focal Adhesion sites

FA sites were segmented using K-means clustering of signals in GFP-FA TIR-FSM images. The low level of GFP-FA protein expression resulting in a punctate instead of continuous labeling of the FAs in FSM images makes it difficult to segment FAs in a single frame of the movie. Therefore, we first integrated the GFP signal for each 10 frame time-step to accumulate a more continuous image of FAs. FA shape and position are relatively stable over this 100s interval. We have avoided differentiating between so called "focal adhesions" and "focal complexes," and smaller, sub-microscopic clusters of integrins and FA proteins, as these terms are as yet not well-defined in the literature. Here we refer to "focal adhesions" to describe all GFP-labeled structures larger than a cluster of a few speckles. Generally, this was equivalent to patches of ~1 x 1 microns or greater.

Correlational qFSM of FA proteins and F-actin

To examine the dependency between the motions of FA protein speckles and F-actin speckles, we analyzed the average velocity of FA and F-actin speckles within individual FAs using scatter plots that pooled data from all cells imaged with the same GFP-FA protein (Fig. 3A & Fig S5A). The slopes and intercepts were calculated by linear least square regression after exclusion of outlier data points falling outside a threshold ellipse. The long and short axes of the ellipse were given by the directions of

the two principal components of the velocity samples. The radii of the axes were set to 3 times the standard deviations of the respective principal components. Importantly, this kind of analysis was possible because the intrinsic variation of FA protein and F-actin speckle speeds between different FAs and time points was significantly larger than the noise level of the motion vectors.

We also measured the coupling between individual FA protein and F-actin speckles in terms of their direction coupling and velocity magnitude coupling within single focal adhesions of one cell (Fig S3C). The direction coupling score (DCS) is measured by $\cos\theta$, (θ: the angle between the FA protein and F-actin speckle vectors within a pair). A score of 1 defines two vectors with identical directionality and a score of -1 defines two vectors that point in opposite directions. To visualize the heterogeneity of directional coupling between FAs and within single FAs (Fig. 3 C-F, Fig S5B-D, Fig. 4) we calculated the DCS on the grid points with 7x7 pixel spacing. DCS values were then interpolated to the pixel grid by B-splines to generate color-coded score maps. Such a score map was generated for each time point, allowing us to analyze the evolution of flow coupling over time (MovieS5 – 12).

The velocity magnitude coupling score (VMCS) is the ratio between the magnitude of the coupled components of F-actin and FA protein speckle motions, minimizing the influence of random fluctuations. The sources of random fluctuation include imaging noise, association and dissociation of fluorophores within a speckle resulting in positional jitter, fluorophore diffusion within a FA, local contractions of the F-actin network which is not coupled to FAs, and/or high-frequency stage and focus shifts. Therefore, a simple speed ratio of an FA protein and F-actin flow vector pair in

each grid point is not accurate because the random fluctuation component can not be separated from individual flow vectors. Instead, we rely on local spatial averaging to reduce the effect of these fluctuations (see Tables S3 and S5 for the difference between speed ratio and VMCS).

Mathematically, the velocity magnitude coupling between two coupled flow vectors

$$V_{\mathrm{FA}} = V_{\mathrm{FA}}^{c} + R_{\mathrm{FA}} \quad \text{(FA flow)}$$
$$V_{\mathrm{act}} = V_{\mathrm{act}}^{c} + R_{\mathrm{act}} \quad \text{(actin flow)}$$

is defined by $\left(V_{\mathrm{FA}}^{c} \bullet V_{\mathrm{act}}^{c}\right) / \left|V_{\mathrm{act}}^{c}\right|^{2}$. The equations indicate that the actual velocity measurements V_{FA} and V_{act} are contaminated by the noise vectors R_{FA} and R_{act} respectively. In the absence of random fluctuations and with perfect coupling, i.e. the coupled components (V_{FA}^{c} and V_{act}^{c}) point in the same direction, the VMCS would equal the measured speed ratio $\left|V_{\mathrm{FA}}\right| / \left|V_{\mathrm{act}}\right|$. In presence of random fluctuations, the best approximation of $\left(V_{\mathrm{FA}}^{c} \bullet V_{\mathrm{act}}^{c}\right) / \left|V_{\mathrm{act}}^{c}\right|^{2}$ is obtained by averaging the measured velocities and calculating the magnitude ratio of the averaged flows. Critically, this procedure is much more robust than averaging the ratios of individual flow vector pairs. Particularly, the fluctuations in the denominator of the ratio propagate unfavorably and bias the estimate systematically. By averaging first, the influence of fluctuations on the ratio calculation is effectively suppressed, assuming that the mean of the random fluctuations is zero. Accordingly, we calculate the average VMCS between two flow vector populations by $\left(E(V_{\mathrm{FA}}) \bullet E(V_{\mathrm{act}})\right) / \left|E(V_{\mathrm{act}})\right|^{2}$, where $E(\bullet)$ denotes the expectation value of the velocity

vectors. In our implementation the expectation value is approximated by the mean of the velocity vectors.

Direct averaging of flow vectors over the entire field of view may, however, underestimate the coupled components. Spatial and temporal heterogeneity between FAs generates flows of diverse directions across the cellular domain (Fig S3D). Indeed, we are interested in capturing this heterogeneity in order to correlate spatiotemporal variability in FA protein/F-actin coupling with dynamic morphological outputs such as cell edge movements. To solve this problem, we first performed a clustering analysis of the F-actin flow population to generate regional clusters of flows of similar directions. The clustering was based on the average direction of local flow vectors (within blocks of 30x30 pixels) so that the difference between local average flow directions within each cluster was less than 30^{O}. We then calculated the average vector of F-actin flows of each cluster and used it as the alignment axis of that cluster. Flow vectors (of both channels) in each cluster were then rotated jointly so that the alignment axes of all clusters pointed in one direction (e.g. Y-axis of the image (Fig.S3E)). Subsequently, population averages of flow vectors per time point were calculated to estimate time-resolved VMCS for each individual cell.

Coherency test and noise control

In this study, we are interested in the transmission of directionally coherent F-actin flow to FA proteins as a measure of FA protein/F-actin coupling. To identify coherent F-actin flow populations, we performed a coherency test on the F-actin flow field at each time-step by evaluating the local coherency of flow vectors within blocks of

30x30 pixels. Each block is assigned a coherency score defined as $\left|(1/N)\sum V_i/|V_i|\right|$, i.e. the magnitude of the vector average of all normalized vectors inside the block ($V_i/|V_i|$: unit flow vector; N : number of vectors within one block). With this definition, the coherency score is 1 if all vectors within the block are parallel and is close to 0 if their directions are random.

To pass the coherency test, the F-actin flow vector population in a block had to satisfy i) the population was greater than 3; ii) the coherency score was above 0.7; iii) the speed was greater than 0.2 pix/frame. Data points within blocks that fail the tests were excluded from the analysis. The threshold of 0.7 for the coherency score and 0.2pix/frame for the speed score were defined empirically based on estimations of the experimental and tracking errors. Specifically, we measured the coherency and the speed of F-actin speckles in fixed cells (cells were injected with x-rhodamine actin, fixed for 20min with 4% formaldehyde in 10mM MES, 3mMMgCl_2, 138mMKCL, 2mMEGTA, then mounted, imaged and analyzed using the same conditions as live cell experiments). The fixed cells had an average coherency score of 0.45 (±0.05, n=4) and an average speed of 0.17pix/frame (±0.04, n=4, 1pix=0.064μm, 1 frame=10sec). Only time points within which 60% or more data points passed the test were retained for analysis. This typically contained ~85% (±9%, SD) of the total data points for each movie. Only movies with an averaged F-actin flow speed above 0.4pix/frame and averaged F-actin flow coherency greater than 0.65 were used in the analysis.

Statistical analysis

For linear regression of FA speckle and F-actin speckle velocities, the correlation

coefficients (r) and their standard deviations were calculated by Bootstrap regression with 200 trials, where each trial generates one independent measurement of correlation coefficient using a dataset randomly resampled from the original data. Each trial dataset has the same sample size as the original data.

One-way-ANOVA and t-test analysis were carried out using the "Analyze-it" statistical package in Microsoft Excel.

For calculating the coupling scores between FA protein and F-actin speckle flows, each cell was treated as an independent event (n=number of cells). Because GFP-FA proteins and x-rhodamine/Alexa-568 actin are incorporated into two different cytoskeletal assemblies, the fluctuation of the correlation between the FA protein and F-actin speckle flow fields is likely to be influenced by cell-to-cell variation.

For comparing the flows between GFP-actin and x-rhodamine/Alexa-568 actin in the same cell, each time-step was treated as an independent event (n=139 time-steps pooled from 8 cells). It is inappropriate to treat each cell as an independent event in this case, because GFP-actin and x-rhodamine/Alexa568 actin are incorporated into the same cytoskeletal assembly. Therefore, the correlation between these two flow fields is expected to be perfect and constant over time regardless of cell behavior. Thus, fluctuation between time points is associated with noise.

For figure representation, box and whisker plots were used. In these plots, boxes indicate the 25% (lower bound), median (middle line) and the 75% (upper bound), whiskers indicate the nearest observations within 1.5 times the interquartile range, notches represent the 95% confidence interval of the median , and + and 0 represent near and far outliers, respectively.

Validation of FA speckle image formation and flow coupling analysis using Monte Carlo simulations of F-actin and FA molecules

To examine speckle image formation in FAs and the effect of protein association/dissociation, diffusion, and camera noise on the apparent speckle velocity in FA proteins that are uncoupled from or transiently coupled to the moving F-actin network, we implemented a Monte Carlo simulation of various molecular motion regimes and investigated how they translate into different speckle dynamics by generating synthetic FSM movies. In the following three sections we describe **i)** the model and the simulation algorithm; **ii)** the results of simulating and analyzing FSM movies of fluorescent FA proteins associating and dissociating with an immobile FA "platform" (i.e. the ECM on the substrate); and **iii)** the results of simulating and analyzing dual-channel FSM movies of fluorescent FA proteins associating and dissociating with both flowing F-actin networks and an immobile FA platform.

Simulation of FSM Movies

We produced synthetic FSM movies of F-actin and FA proteins in one or two channels using a Monte Carlo approach. Two-color movies of F-actin and FA protein flow are a composite of two independently produced single-channel movies, each generated by using specific parameters of F-actin turnover and flow (*S12*) or FA protein turnover (our own unpublished FRAP data). For all synthetic movies, we set the frame rate to 10 s per frame, camera exposure time to 800 ms, NA to 1.45, and pixel size in object space to 64 nm, all in accordance with the parameters of our live-cell experiments.

Simulations started by initializing a field of randomly distributed fluorescent proteins labeled with a single fluorophore, each assigned a state. In models of F-actin networks, fluorescent proteins can be in either of the following states: 1) unbound; or 2) bound to the network, where the fluorescent protein moves with a constant velocity v (0.25 μm/min for all simulations, in accordance with measured F-actin lamella flow in PtK1 cells (*S13*)). In models of FAs, fluorescent proteins can be in one of four states (Fig S6): 1) unbound; 2) immobilized by binding to the FA platform; 3) bound to the F-actin network, i.e. the fluorophore moves with velocity v; 4) bound to both FA platform and F-actin network. Although it is likely very physiologically important, there is no experimental data that describes the exact nature of this fourth state. Furthermore, at the time scale of our simulations (100 ms), this state is very transient when we estimate it based on association and dissociation rate constants measured in FSM and FRAP experiments. Thus, we neglected state 4 in the practical implementation of the Monte Carlo simulations. Importantly, with these three states, a fluorescent FA protein in an FA speckle can either be stationary or move with velocity v. One of the goals of these simulations was to determine how the apparent velocity of F-actin speckles tracked in FSM movies relates to the association and dissociation rates of fluorescent FA proteins in these states. We also created the option of simulating diffusional movement of FA proteins while bound to the FA platform, representing diffusion of molecules within the FA, to test how random positional jitter of different magnitudes affects the measurements.

Fluorescent proteins transition between states with a probability determined by the rate constants for fluorescent protein association and dissociation from the F-actin

network and FA platform, and the time-step used for the Monte Carlo simulation. In simulations of F-actin, only two constants are relevant: the k_{on} and k_{off}, denoted k_{on12} and k_{off21} (Fig S6). In simulations of FA, we assumed that the rates of the two possible transitions to state 2 (k_{on12} and k_{on32}) are equal. The same holds for the rates of the transitions to state 3 (k_{on13} and k_{on23}). The dissociation rates from states 2 and 3 back to state 1 (k_{off21} and k_{off31}) are independent.

At each time-step, the probability P of changing to a new state (P=k*dT) is compared to a random number R drawn from a uniform distribution to determine if a transition between states will occur. For F-actin simulations, a fluorescent monomer undergoes a state change if P/R > 1. For FA simulations, where a fluorescent FA protein can transition to two states, the maximum ratio P/R is considered. The fluorescent FA protein undergoes a state change if max(P/R) > 1. For both F-actin and FA simulations, if no transition yields P/R > 1, the state remains unchanged.

After every 10 s of simulation time, an image is "recorded." To simulate an 800 ms exposure time, the intensities of fluorescent proteins are summed over eight 100-ms time-steps. Subsequently, a Gaussian approximation of the 2D point spread function of the microscope is used to generate diffraction-limited images (*S14*). These are then re-sampled from nanometers to pixels according to the pixel size in object space.

Recording the x,y-positions and states for all fluorescent proteins over time allows the measurement of the turnover time $T_{1/2}$ as a function of the association and dissociation rate constants. We define $T_{1/2}$ as the amount of time it takes for half the bound fluorescent proteins to become unbound. In agreement with the theory of FRAP analyses, we found that $T_{1/2}$ did not depend on k_{on} but was inversely proportional to k_{off}.

We chose rate constants to yield turnover times that matched experimentally determined turnover times: For example, $k_{off} = 0.02$ translates into $T_{1/2} \sim 35$ s, which is close to that of x-rhodamine F-actin (~50 s); $k_{off} = 0.005$ translates into $T_{1/2}$ of ~140 s, which is similar to that of GFP-vinculin (~185 s, both unpublished FRAP measurements in PtK1 cells).

An important property of our simulations is that for a given set of rate constants, a steady state is reached regardless of the initial distribution of states. Thus, independent of whether all fluorescent proteins are initially unbound (state 1) or bound to the F-actin network or FA platform (state 2), after a certain period of time the ratio between the states will be constant. The time it takes to reach steady state depends on the magnitude of the rate constants. All velocity and flow coherency measurements shown in the following sections were made under steady state conditions. Similarly, we measured $T_{1/2}$ only after reaching steady state.

Simulation of FSM Movies of Platform-bound FA Proteins

First, we used our simulation framework to test in a stationary FA whether fluorescent protein association and dissociation, camera noise, or molecular diffusion could yield a speckle flow field similar to what we observed in our imaging experiments (Fig. 2). We generated movies of fluorescent FA proteins switching between state 1 (unbound) and state 2 (bound to the FA platform) with five different levels of protein diffusion when bound to the FA platform (Fig S7A; movieS13). For each diffusion level, we tested the following conditions: i) no fluorescent protein association/dissociation, no camera noise; ii) no fluorescent protein association/dissociation, but added camera noise resulting in a SNR = 2; iii) fluorescent protein association/dissociation with $T_{1/2} \sim 35$ s, no camera noise; and iv) both fluorescent protein association/dissociation and camera

noise (SNR = 2). Coherent F-actin flow (0.25 μm/min) was also simulated to allow computation of the VMCS and DCS with the diffusing FA protein. However, in this simulation FA proteins never switched to state 2 where they would interact with the flowing F-actin. All simulated FSM movies were tracked and analyzed following the same procedures applied to experimental movies of living cells.

Fig S7 and movie S13 show the results for five levels of protein diffusion, analyzed using condition (iii) for D = 10^{-9}cm^2/s, which approximates free protein diffusion in membrane (see (*S15*)), and condition (iv) for all other diffusion constants. For all values of D, FA protein speckle motions induced by diffusion, turnover and noise were oriented in random directions and produced no apparent coupling to the simulated coherent F-actin flow, which runs from the left to the right image border (not shown). In particular, at the free membrane diffusion speed (D=10^{-9}cm^2/s), fluorescent FA proteins were moving too quickly (~31 pixels per frame) to form speckles during the 800 ms exposure time. Thus, there were few stable image features that allowed for reliable motion tracking at the 10 s frame rate. Note the abundance of red circles in the D=10^{-9}cm^2/s panel in Fig S7B, which indicate points rejected by the software as untrackable (*S10*). By comparing this to the rejection rate in experimental movies, we conclude that FA proteins are much less diffusive while bound to FAs in vivo. At more realistic, slower diffusion levels (<10^{-11}cm^2/s), the detected FA speckle motion due to association/disassociation and camera noise was very small and random as indicated by the low coherency score (~0.3 as compared to 0.7 or greater for actin-binding FA proteins and ~0.5 for integrins and FA core proteins; see Table S1). At these diffusion levels, both the VMCS and the DCS values with F-actin were at least one order of magnitude

below the scores measured experimentally (compare Fig S7A to Tables S4 and S5). Therefore, fluorescent protein diffusion within FAs, turnover and noise does not produce a speckle motion that would falsely indicate coupling between an FA protein and a flowing F-actin network.

Simulations with Variable Transient Coupling Between FA Proteins and F-actin

Second, we tested how changes in the rates of association and dissociation of FA proteins interacting with either the FA platform or the F-actin network affect the coupling scores measured in synthetic dual-channel FSM movies, and whether changes in these scores are faithful indicators of differential coupling between FA proteins and the F-actin network. We generated 25 synthetic FSM movies in which we systematically varied the association rates in the FA protein channel. To simplify the parameter space, we varied the k_{on} to the FA platform (state 2) ($k_{on2} = k_{on12} = k_{on32}$) and the k_{on} to F-actin (state 3) ($k_{on3} = k_{on13} = k_{on23}$) and set k_{off} ($k_{off21} = k_{off31}$) to 0.005. This achieved a T1/2 ~140 s, in agreement with FRAP measurements of GFP-vinculin turnover in FAs (unpublished). The velocity of F-actin flow was 0.25 μm/min.

VMCSs were calculated after tracking both the simulated F-actin and FA protein speckle fields (Fig S8A; movieS14). In accordance with our interpretation of the VMCS for experimental data, a low degree of coupling (high k_{on2} to the FA platform and low k_{on3} to F-actin) yields a VMCS close to 0, whereas a high degree of FA protein coupling to F-actin (low k_{on2} to FA platform and high k_{on3} to F-actin) yields a VMCS close to 1. FigS8B displays selected examples from this parameter space with increasing coupling from the left to the right panels. FigS8C presents a plot of VMCS versus $R_{kon} = k_{on3}/(k_{on2}+k_{on3})$, where R_{kon} reflects the fraction of total FA proteins bound to F-actin.

The two variables have an almost perfect linear relationship. At low values of R_{kon}, only a few FA proteins translocate with the F-actin network, which is reflected in low FA speckle velocities and, importantly, low VMCS. As the fraction of FA proteins traveling with the F-actin network increases, the FA speckle velocities and VMCS values increase. Thus, the VMCS is a consistent estimate of the degree of coupling of an FA molecule to the F-actin network.

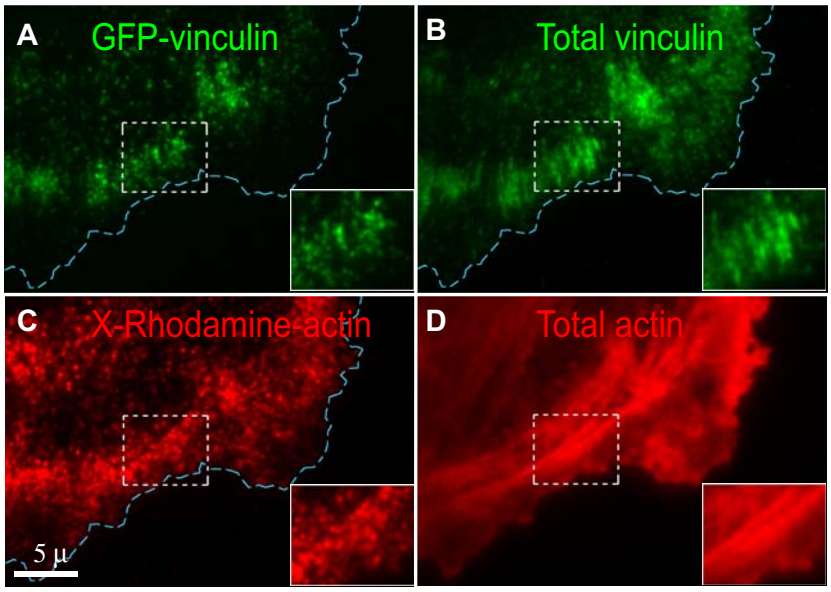

Figure S1. TIR-FSM imaging of F-actin and FAs.
In FSM, a non-uniform pattern of fluorophores is generated in macromolecular structures whose subunit size is below the level of resolution of the light microscope. The fluorophore pattern arises by assembly of the structure from a subunit pool with a very low ratio of fluorescent:non-fluorescent subunits. In high-resolution fluorescence images, fluorophore clusters in the structure are detected as local intensity maxima called speckles (Fig 1A). Speckle dynamics over time encode kinetic (turnover) and kinematic (motion) information about the dynamics of sub-resolution subunits within the structure (S2, S11, S13, S16, S17). To reveal molecular dynamics within FAs, we combined FSM with total internal reflection fluorescence (TIRF) microscopy. In TIRF microscopy, an evanescent field is generated at a coverslip/cell interface when light is introduced to this interface at a critical angle. The thin (50-200 nm) evanescent field can be used to excite fluorophores close to this interface, thus optimizing speckle contrast by eliminating the contribution from cytoplasmic fluorescence outside the evanescent field (S4). A,C) TIRF images of a PtK1 cell expressing a low level of GFP-vinculin and injected with low level of Alexa568-actin that sparsely labels FAs (A) and the F-actin cytoskeleton (C) resulting in a speckled fluorescence distribution within the structures. B,D) TIRF images of the same cell, fixed and immunofluorescently labeled with anti-vinculin antibodies and stained with Alexa-568-phalloidin to visualize total vinculin (B) and total F-actin (D), resulting in a relatively continuous labeling of the structures. Dashed boxed areas are zoomed in the insets.

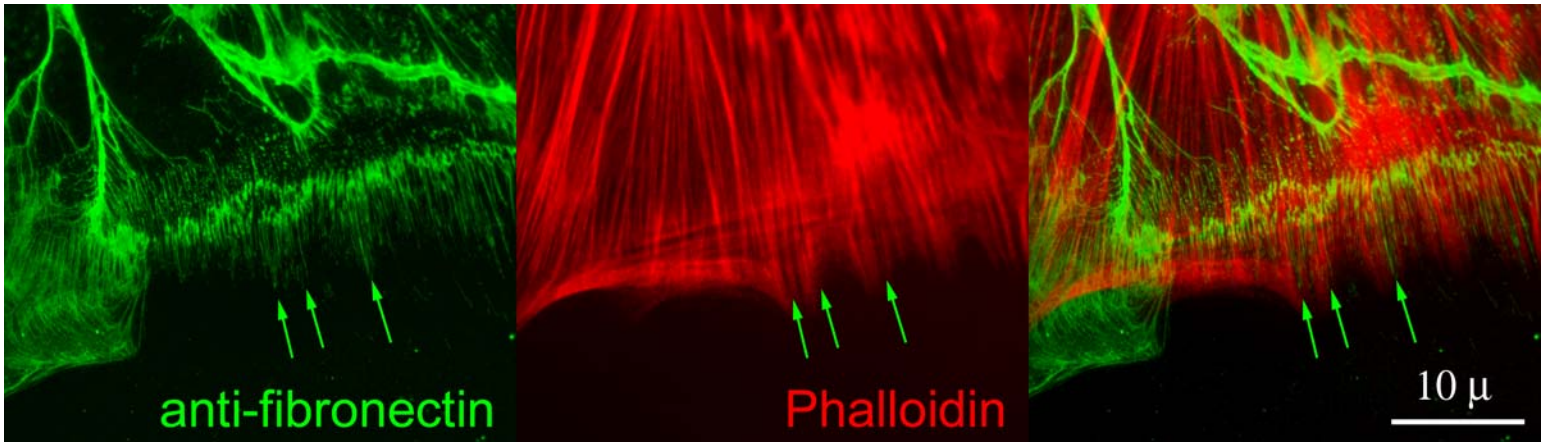

Figure S2. Ptk1 cells organize a fibronectin-containing ECM on glass coverslips. Localization of fibronectin and F-actin in Ptk1 cells plated on a glass coverslip in serum-containing medium for 2 days. Fibronectin was immunolabeled with anti-fibronectin antibody (green) and F-actin was labeled with Alexa-568-phalloidin (red). Fibronectin fibrils often coaligned with F-actin bundles in the lamella (arrows), similar to what has been observed in fibroblasts (S18).

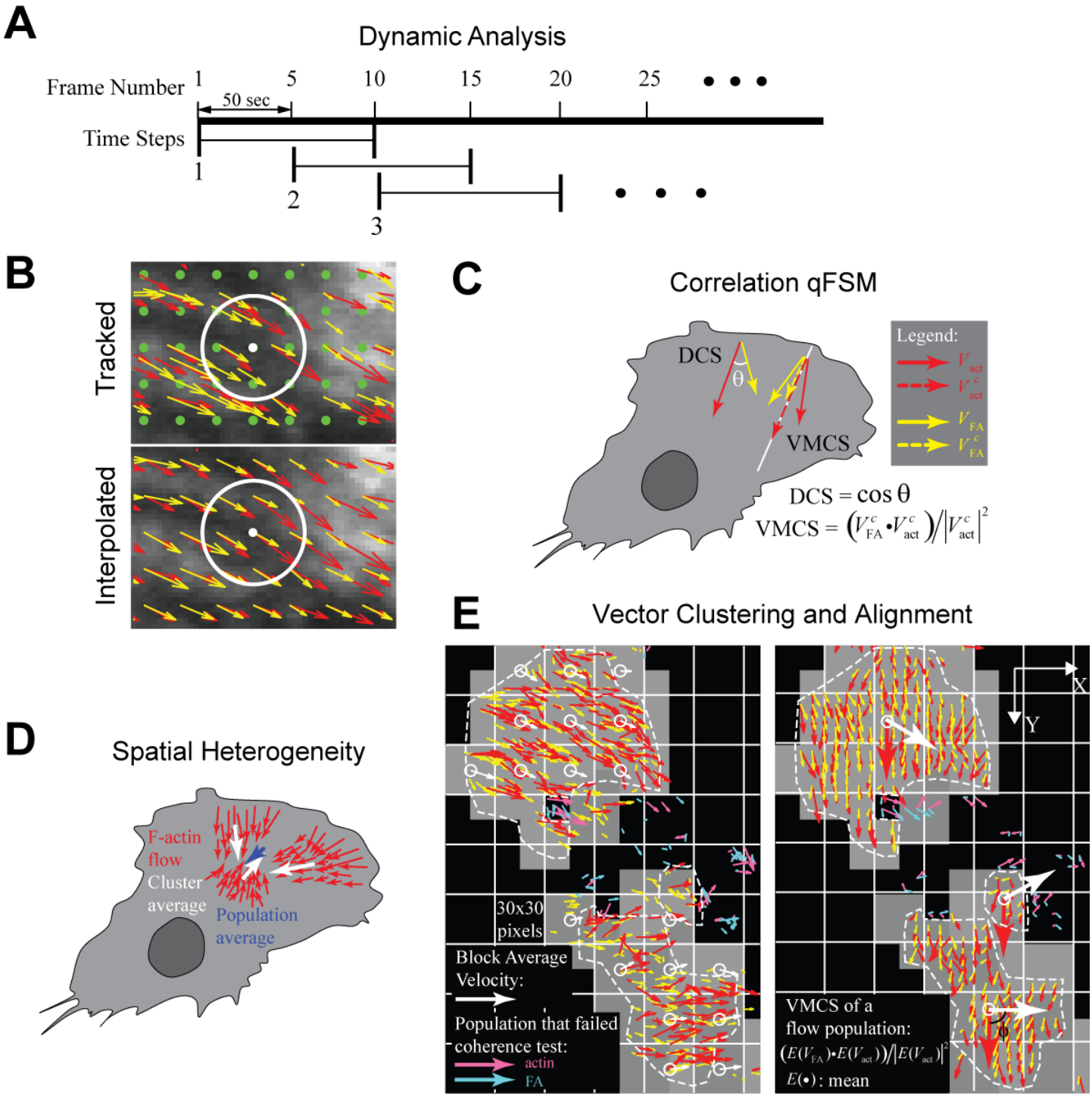
A
Dynamic Analysis
Frame Number
1
5
10
15
20
25
50 sec
Time Steps
1
2
3
B
Tracked
Interpolated
C
Correlation qFSM
DCS
θ
VMCS
Legend:
V_{act}
V^c_{act}
V_{FA}
V^c_{FA}
$DCS = \cos\theta$
$VMCS = \left(V^c_{FA} \cdot V^c_{act}\right) / \left|V^c_{act}\right|^2$
D
Spatial Heterogeneity
F-actin flow
Cluster average
Population average
E
Vector Clustering and Alignment
30x30 pixels
Block Average Velocity:
Population that failed coherence test:
actin
FA
X
Y
VMCS of a flow population:
$(E(V_{FA}) \cdot E(V_{act})) / |E(V_{act})|^2$
$E(\bullet)$: mean
ϕ

Figure S3. Illustration of image analysis methods in Correlation qFSM.

A) Motions of F-actin and FA protein speckles in the same cell were tracked using a multi-frame cross-correlation technique at overlapped time windows of 10 frames each. This allowed us to study variations in the correlation of F-actin and FA protein motions within FAs at a time scale of ~100 sec. B) The vectors representing tracked F-actin and FA protein speckle motions were interpolated to a common grid (7x7 pixels) so that the correlation of two vectors could be directly calculated at the same positions. We used a distance weighted average based on a Gaussian kernel with a radius of ~11 pixels (white circles) to calculate the interpolated velocities. C) Two scores were defined to measure the degree of correlation between the two flow fields: i) Direction Coupling Score (DCS) defined as $\cos\theta$, where θ is the angle between the F-actin and FA flow vectors; ii) Velocity Magnitude Coupling Score (VMCS) defined as $\left(V_{\mathrm{FA}}^{c} \bullet V_{\mathrm{act}}^{c}\right) \Big/ \left|V_{\mathrm{act}}^{c}\right|^{2}$ where V_{FA}^{c} and V_{act}^{c} (dotted arrows) are the coupled components of the flow vectors. In the presence of random fluctuations, V_{FA}^{c} and V_{act}^{c} can not be identified for individual vector pairs. We relied on averaging to reduce the effect of noise and calculate the average VMCS for a specific flow population by $\left(E(V_{\mathrm{FA}}) \bullet E(V_{\mathrm{act}})\right) \Big/ \left|E(V_{\mathrm{act}})\right|^{2}$ where $E(\bullet)$ denotes the mean. D) Due to intrinsic spatial heterogeneity of flow directions across the observed cellular domain, calculation of the mean of the actin flow velocities can cancel out the true local velocity (as illustrated by an extreme example in the cartoon). We therefore performed a clustering and alignment of the flow vectors prior to calculating their mean, as illustrated in (E). E) Clusters of vectors with similar directions were identified and aligned before calculating their mean. The clustering of similar actin flow directions ($< 30^{0}$) was based on the local average velocity of the F-actin flow within a 30x30 pixels box. The flow vectors in each cluster were then rotated by a common angle

so that the cluster average velocity of the F-actin flow was aligned with the Y-axis. The white arrow centered at each cluster denotes the average F-actin flow axis before rotation, whereas the red arrow denotes the average after rotation, and ϕ the common angle. Flow velocities that failed a coherency and speed threshold test (vectors in black boxes) were excluded from the correlation analysis.

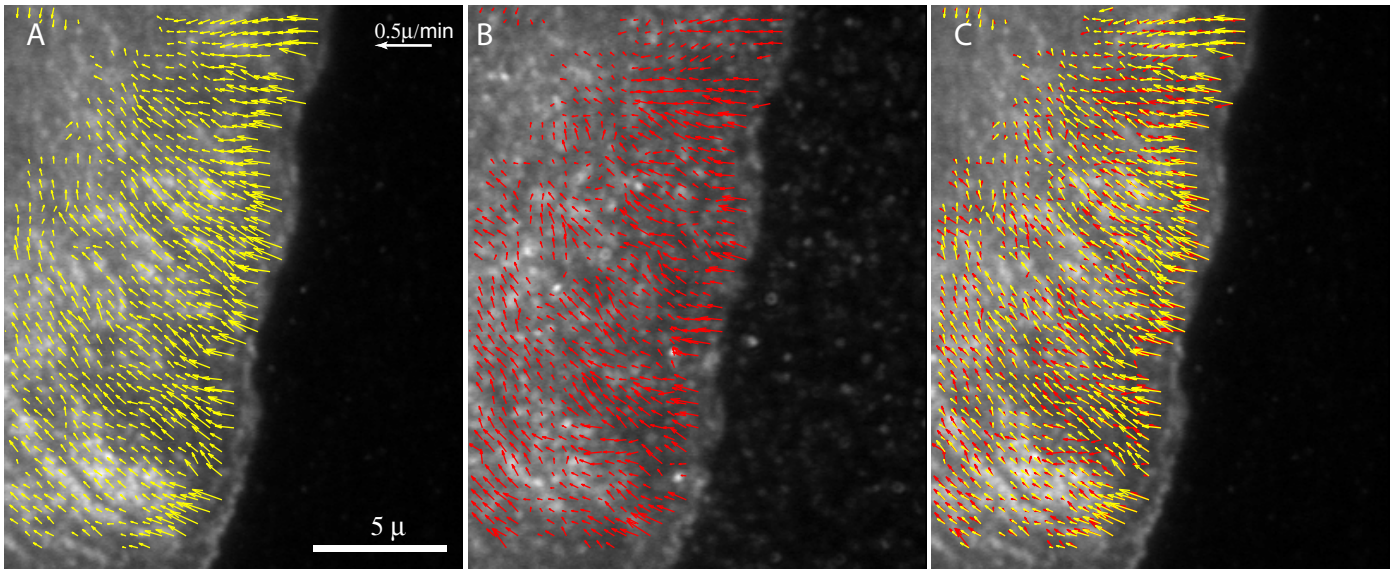

Figure S4. Tracking GFP-actin and Alexa568-actin in the same cell yields similar F-actin flow maps.

A cell was co-microinjected in the nucleus with plasmid encoding GFP actin and Alexa568-actin protein and imaged as for cells containing labeled FA protein and actin. F-actin speckles were tracked separately in both channels, and flow maps from the two channels interpolated onto a grid. Correlational analysis was then performed.

Interpolated vector maps of GFP-actin (A, yellow vectors) and Alexa568-actin (B, red vectors) speckles are shown. As expected, the two F-actin flow fields are very similar. However, the flow fields of GFP-actin are slightly but significantly more coherent (coherency =0. 89 $\pm$0.01, $P<0.0001$, n=139 timesteps) and faster (speed= 0.27$\pm$ 0.01μm/min, P=0.002, n=139 timesteps) than for cytochemically labeled actin (coherency =0.82 $\pm$ 0.01, speed=0.24 $\pm$ 0.01μm/min) (also see movieS4). Although the two flow fields are highly correlated in direction and velocity (DCS= 0.882$\pm$ 0.009, VMCS= 1.13$\pm$0.03), they deviate from 1 by slightly over 10%, indicating systematic errors that result in slight under-estimation of the DCS and over-estimation of the VMCS. Two properties of the cytochemically labeled actin protein could contribute to this effect: 1) cytochemically labeled actin monomers might be mixed with a small amount of free fluorophores, which, when injected into the cell, increases the cytoplasmic background and degrades the signal:noise ratio of F-actin speckles and the precision of tracking; and 2) cytochemically labeled actin tends to stick to the coverslip, which appears as stationary speckles in the flow fields, thus decreasing the average speed and increasing the noise in direction measurements of the vectors. In addition, imaging system noise or drift and speckle tracking errors also contribute to the error.

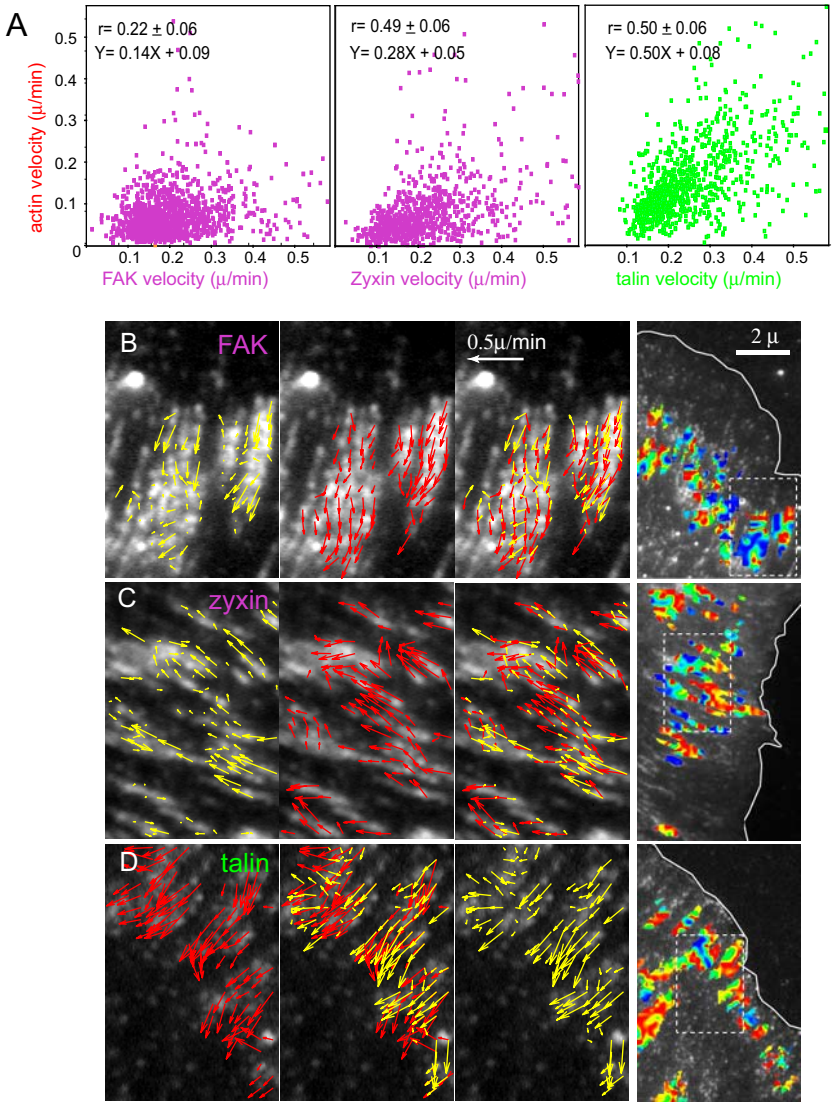

Figure S5. Additional FA proteins analyzed by correlational FSM.
A) Scatter plots of FA protein speckle motion (X-axis) vs F-actin speckle motion (Y-axis) for GFP conjugates of zyxin, FAK and talin. The position of each data point represents the averaged FA protein speckle velocity and the corresponding F-actin speckle velocity over one FA. The correlation coefficients (r) and 2X standard deviations were calculated by Bootstrap regression with 200 trials. B-D) Shown from left to right in each panel are the FA flow vector maps, the corresponding F-actin flow vector maps, overlay of the two, color coded direction correlation maps (in lower magnification) of 3 GFP-tagged FA proteins: zyxin, FAK and talin.

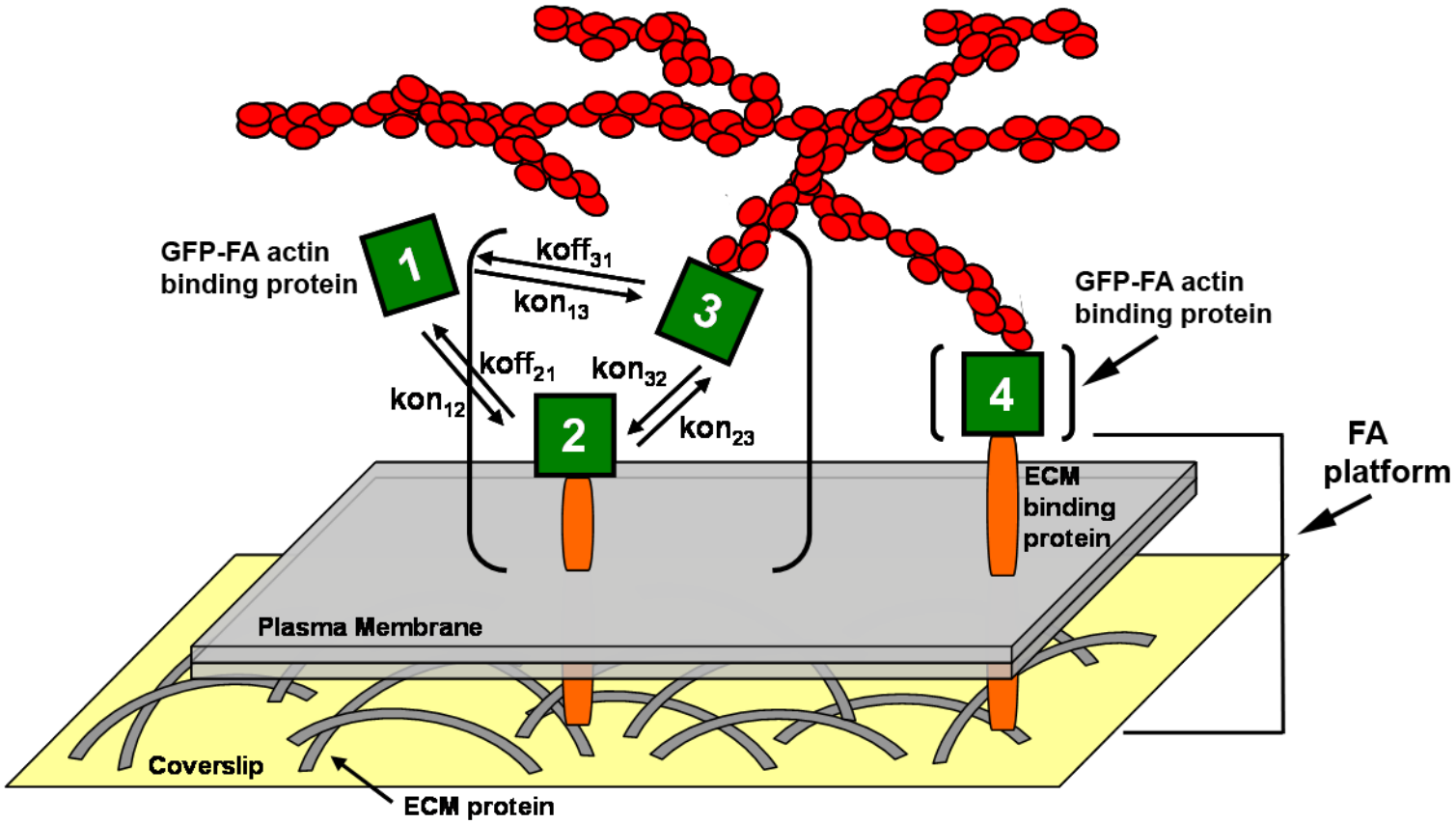

Figure S6. Definition of states and state transitions for FA proteins considered in the Monte Carlo simulation.
State 4 corresponds to a transient state where the FA protein is bound to both the FA platform and F-actin, either directly or indirectly. Because the timescale of these interactions is assumed to be short compared to the frame rate and exposure time, we did not include state 4 in the present model.

A.

Measured FA protein speckle dynamics due to association/dissociation and noise in simulated FSM movies					
Diffusion constant (cm^2/sec)	**1.00E-09**	**1.00E-11**	**1.00E-12**	**1.00E-15**	**0.00E+00**
Turnover $T_{1/2}$ (sec)	**34.70**	**33.70**	**34.30**	**34.69**	**35.16**
Mean fluorophore speed (μm/min)	12.00	1.20	0.38	0.01	0.00
Mean speckle speed (μm/min)	1.31	0.30	0.05	0.03	0.01
Coherence score	0.55	0.44	0.34	0.33	0.27

Measured FA protein/F-actin speckle coupling in simulated FSM movies where k_{on13} and k_{on23} = 0					
VMCS (Velocity Magnitude Coupling Score)	-0.6248	0.0639	-0.0146	0.0132	-0.0065
DCS (Direction Coupling Score)	-0.064	0.0551	-0.0641	0.0981	-0.0921
Mean speed ratio (FA:F-actin)	5.26	1.19	0.21	0.11	0.05

All adhesion movies have SNR = 2 and $k_{on12} = k_{off21} = 0.02$. F-actin speckle flow velocity was 0.25μm/min in all conditions.

B.

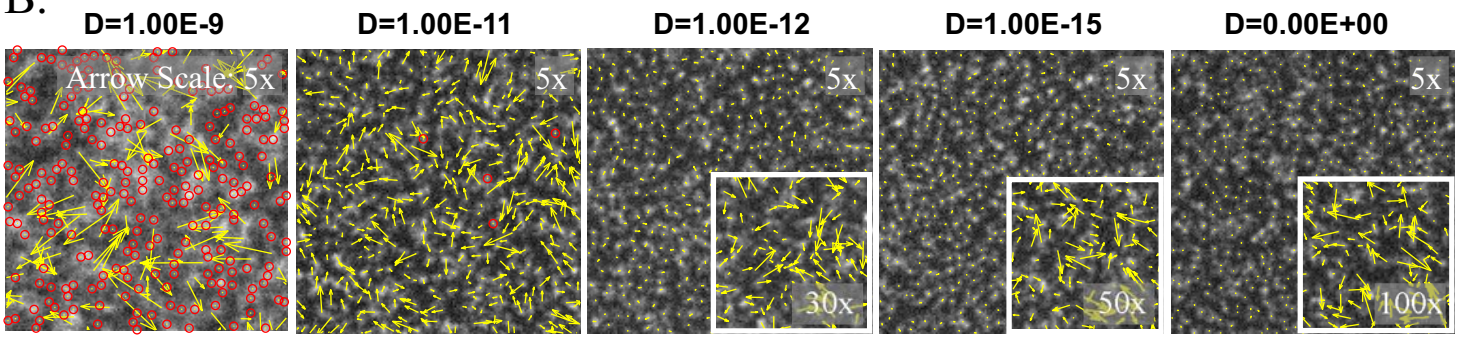

Figure S7. Effect of diffusion, FA protein association and dissociation and camera noise on motion tracking and coupling analysis of FA proteins in Monte Carlo simulations.
A) Speed measurements and coupling scores for the five diffusion conditions used in the Monte Carlo simulation of the FA proteins (see also movieS13). FA proteins switched between unbound and FA platform-bound states and did not associate with F-actin. For all diffusion levels, coherency was below 0.6, the level considered significant in experimental movies. The large mean speckle speed for the highest diffusion constant was a tracking artifact due to instability of the few image features falsely detected as speckles. The speed of speckles in the case of the second highest diffusion constant represents true tracks of diffusive speckle motions. The VMCS and DCS were calculated using simulated dual channel FSM movies of FA speckles and a flowing F-actin speckle field (from left to right) in which FA proteins could only switch between unbound and FA platform-bound states, but could not associate with F-actin. The scores indicate that there could be no significant apparent coupling occurring due to diffusion, FA protein association and dissociation and camera noise. B) Tracked motion of the simulated FA protein speckles (yellow vectors scaled at 5X) shows random fluctuation at the five diffusion levels listed in (A). Insets show vectors magnified by the amount indicated. Red circles are points marked as untrackable by the cross-correlation tracking algorithm. For a diffusion constant D = 1.00E-9cm2/s, corresponding to free protein diffusion in a membrane, the abundance of untrackable points reveals that image features are unstable at a frame interval of 10 s/frame (left-most panel).

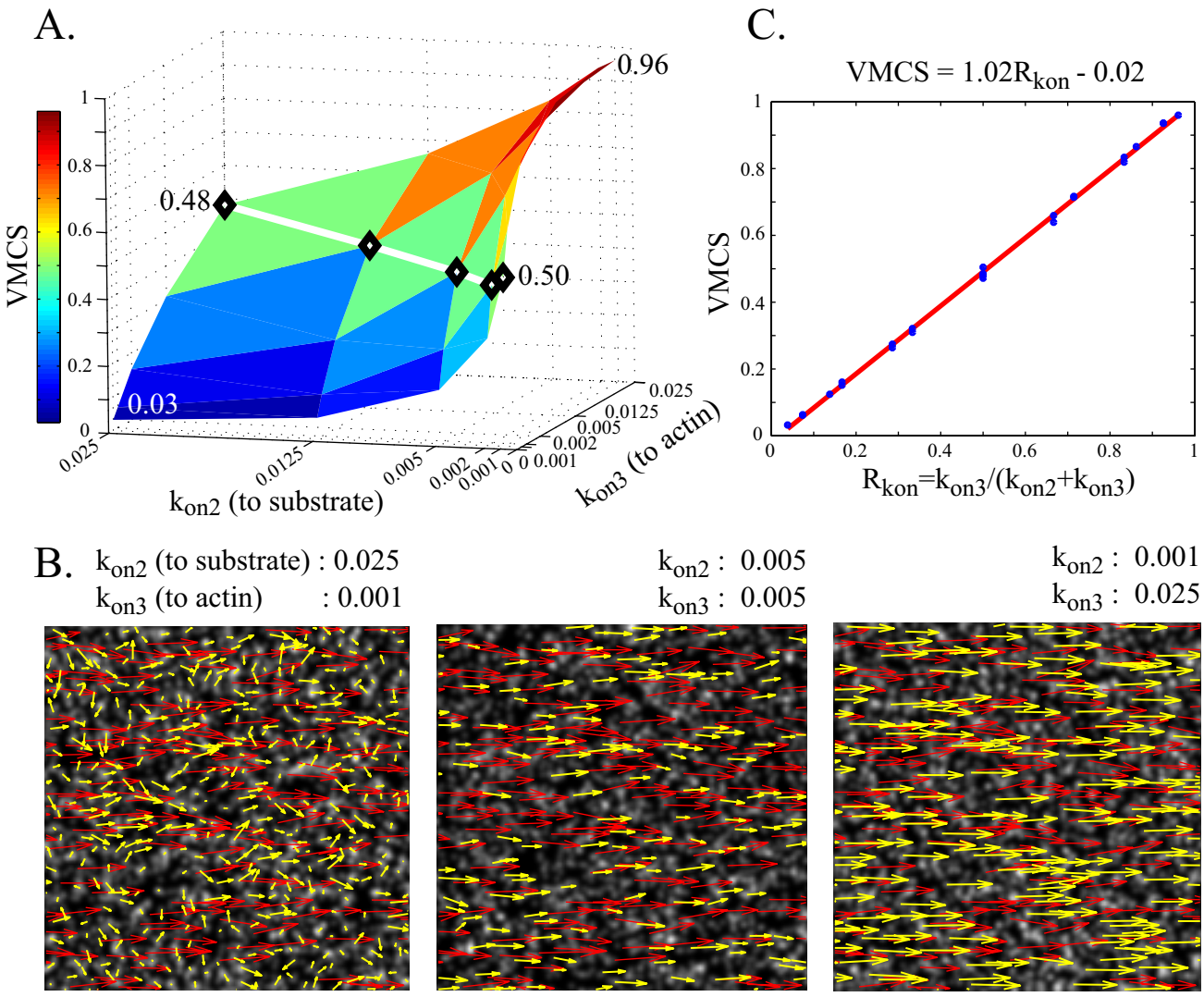

Figure S8. Varying the association and dissociation rate constants of FA proteins in Monte Carlo simulations affects the speed of FA speckle motion and the coupling to F-actin.
In these simulations, FA proteins switched between unbound (1), FA platform-bound (2), and F-actin-bound (3) states to allow coupling to F-actin flow. The VMCS and DCS were calculated using a simulation of F-actin flowing from left to right at v = 0.25 μm/min. A) Surface plot of VMCS determined by tracking 25 simulated FSM movies with the same dissociation rate constant (k_{off} = k_{off21} = k_{off31} = 0.005) and variable association rate constants to the FA platform (k_{on2}) and to F-actin (k_{on3}). In the five FSM movies where k_{on2} equals k_{on3} (black diamonds), the VMCS was ~0.5, in agreement with the notion that half the FA proteins are stationary while the other half move at v. B) Tracked motion of FA speckles (yellow vectors) for three representative FSM movies out of the 25. VMCS increased from left to right as FA protein speckle flow became more aligned with F-actin speckle flow and more FA proteins were bound to the F-actin network. C) Scatter plot of VMCS versus R_{kon} = $k_{on3}/(k_{on2}+k_{on3})$. Rkon is a measure of the fraction of total FA proteins bound to F-actin.

Supplemental Tables and Legends:

Table S1: FA protein speckle coherency scores. Average motion coherency of speckles in FA of cells expressing each GFP-tagged FA protein was computed. Coherency measures the directional variability in adjacent vectors (See Materials and Methods). n: number of cells; each cell contains ~2,000-10,000 data points and 10-32 time-steps (one time-step = motion integrated over 10 frames captured at 10s/frame). SEM: Standard Error of the Mean; $P_{X/}$: P value of pair-wise t-test or One-way ANOVA; Bold lettering: P values below 0.05, i.e. the coherency scores are significantly different between speckle motions of two FA molecules (pair-wise t-test) or among those of a group of FA molecules (One-way ANOVA).

		Integrin	FA core proteins			FA actin-binding proteins		
FA molecule	Mean±2SEM	$P_{alphaV/}$	$P_{FAK/}$	$P_{zyxin/}$	$P_{paxillin\ /}$	$P_{vinculin/}$	$P_{talin/}$	$P_{actinin/}$
α_V/β_3(n=5)	0.47±0.04							
FAK(n=5)	0.48±0.05	0.83						
Zyxin(n=4)	0.57±0.08	0.07	0.10					
Paxillin(n=6)	0.52±0.04	0.11	0.21	0.28				
Vinculin(n=9)	0.75±0.07	**0.0001**	**0.0002**	**0.01**	**0.0003**			
Talin(n=4)	0.64±0.07	**0.003**	**0.006**	0.20	**0.01**	0.11		
α-actinin(n=4)	0.84±0.02	**<0.0001**	**<0.0001**	**0.0007**	**<0.0001**	0.12	**0.002**	
One-way ANOVA		**P_{all7} <0.0001**						
			P_{FAcore} = 0.14					
						$P_{FAactin}$ = 0.02		

Table S2: FA protein speckle speeds. Average speed (in μm/min) of speckles in FA of cells expressing each GFP-tagged FA protein was computed. n: number of cells; each cell contains ~2,000-10,000 data points and 10-32 time-steps. SEM: Standard Error of the Mean; $P_{X/}$: P value of pair-wise t-test; Bold lettering: P values below 0.05.

		Integrin	FA core proteins			FA actin-binding proteins		
FA molecule	Mean±2SEM (μm/min)	$P_{alphaV/}$	$P_{FAK/}$	$P_{zyxin/}$	$P_{paxillin/}$	$P_{vinculin/}$	$P_{talin/}$	$P_{actinin/}$
α_V/β_3 (n=5)	0.085±0.004							
FAK(n=5)	0.14±0.04	**0.03**						
Zyxin(n=4)	0.11±0.04	0.23	0.30					
Paxillin(n=6)	0.09±0.01	0.27	**0.04**	0.43				
Vinculin(n=9)	0.12±0.03	0.07	0.46	0.55	0.12			
Talin(n=4)	0.21±0.08	**0.01**	0.15	0.06	**0.01**	**0.02**		
α-actinin(n=4)	0.27±0.05	**0.0001**	**0.01**	**0.003**	**<0.0001**	**0.0002**	0.28	
One-way ANOVA		**P_{all7} <0.0001**						
			P_{FAcore} = 0.11					
						$P_{FAactin}$ = 0.001		

Table S3: Ratio of speeds of FA protein and F-actin speckles within FA. To derive the mean, the ratios of the average FA speckle speed and F-actin speckle speed were first calculated for each cell independently. Then these ratios were averaged over multiple cells. n: number of cells; each cell contains ~2,000-10,000 data points and 10-32 time-steps. SEM: Standard Error of the Mean; $P_{X/}$: P value of pair-wise t-test; Bold lettering: P values below 0.05.

		Integrin	FA core proteins			FA actin-binding proteins			actin
FA molecule	Mean±2SEM	$P_{alphaV/}$	$P_{FAK/}$	$P_{zyxin/}$	$P_{paxillin/}$	$P_{vinculin/}$	$P_{talin/}$	$P_{actinin/}$	$P_{actin/}$
α_V/β_3 (n=5)	0.39±0.04								
FAK(n=5)	0.64±0.2	**0.04**							
Zyxin(n=4)	0.44±0.1	0.38	0.16						
Paxillin(n=6)	0.39±0.04	0.94	**0.03**	0.32					
Vinculin(n=9)	0.51±0.06	**0.03**	0.15	0.29	**0.01**				
Talin(n=4)	0.78±0.05	**<0.0001**	0.28	**0.002**	**<0.0001**	**0.0003**			
α-actinin(n=4)	0.99±0.10	**<0.0001**	**0.03**	**0.0003**	**<0.0001**	**<0.0001**	**0.01**		
actin(n=8)	1.13±0.08	**<0.0001**	**0.004**	**<0.0001**	**<0.0001**	**<0.0001**	**0.0003**	0.07	
One-way ANOVA		**P_{all7} <0.0001**							
			P_{FAcore} = 0.04						
						$P_{FAactin}$ <0.0001			

Table S4: Direction Coupling Score (DCS) for FA protein and F-actin speckles within FA. DCS is the average of cosθ, where θ denotes the angle between paired FA protein and F-actin speckle vectors. n: number of cells; each cell contains ~2,000-10,000 data points and 10-32 time-steps. SEM: Standard Error of the Mean; $P_{X/}$: P value of pair-wise t-test; Bold lettering: P values below 0.05.

		Integrin	FA core proteins			FA actin-binding proteins			actin
FA molecule	Mean±2SEM	$P_{alphaV/}$	$P_{FAK/}$	$P_{zyxin/}$	$P_{paxillin/}$	$P_{vinculin/}$	$P_{talin/}$	$P_{actinin/}$	$P_{actin/}$
α_V/β_3 (n=5)	0.32±0.10								
FAK(n=5)	0.26±0.12	0.52							
Zyxin(n=4)	0.47±0.12	0.09	**0.05**						
Paxillin(n=6)	0.36±0.08	0.54	0.23	0.16					
Vinculin(n=9)	0.73±0.08	**<0.0001**	**<0.0001**	**0.005**	**<0.0001**				
Talin(n=4)	0.60±0.15	**0.01**	**0.01**	0.21	**0.01**	0.13			
α-actinin(n=4)	0.84±0.02	**<0.0001**	**<0.0001**	**0.001**	**<0.0001**	0.11	**0.02**		
actin(n=8)	0.87±0.04	**<0.0001**	**<0.0001**	**<0.0001**	**<0.0001**	**0.01**	**0.001**	0.40	
One-way ANOVA		**P_{all7} <0.0001**							
			P_{FAcore} = 0.08						
						$P_{FAactin}$= 0.04			

Table S5: Velocity Magnitude Coupling Score (VMCS) for FA protein and F-actin speckles within FA. VMCS measures the relative motion of FA speckles along the local F-actin flow axis, defined as $\left(E(V_{FA})\bullet E(V_{act})\right)/\left|E(V_{act})\right|^2$ ($E(\bullet)$ denotes the mean velocity). n: number of cells; SEM: Standard Error of the Mean; $P_{X/}$: P value of pair-wise t-test; Bold lettering: P values that below 0.05.

		Integrin	FA core proteins			FA actin-binding proteins			actin
FA molecule	Mean±2SEM	$P_{alphaV/}$	$P_{FAK/}$	$P_{zyxin/}$	$P_{paxillin/}$	$P_{vinculin/}$	$P_{talin/}$	$P_{actinin/}$	$P_{actin/}$
α_V/β_3 a(n=5)	0.17±0.05								
FAK(n=5)	0.26±0.12	0.22							
Zyxin(n=4)	0.32±0.08	**0.02**	0.5						
Paxillin(n=6)	0.21±0.04	0.31	0.37	**0.03**					
Vinculin(n=9)	0.48±0.08	**0.0003**	**0.01**	**0.04**	**0.0003**				
Talin(n=4)	0.59±0.08	**<0.0001**	**0.003**	**0.003**	**<0.0001**	0.12			
α-actinin(n=4)	0.98±0.09	**<0.0001**	**<0.0001**	**<0.0001**	**<0.0001**	**<0.0001**	**0.0006**		
actin(n=8)	1.13±0.04	**<0.0001**	**<0.0001**	**<0.0001**	**<0.0001**	**<0.0001**	**<0.0001**	0.11	
One-way ANOVA		**P_{all7} <0.0001**							
			P_{FAcore} = 0.23						
						$P_{FAactin}$<0.0001			

Supplementary Movie Legends

Supplementary movie 1.

TIR-FSM time-lapse movie of α_v-$\beta_3$integrin-GFP.

Supplementary movie 2.

TIR-FSM time-lapse movies of three FA core proteins tagged with GFP: FAK, zyxin and paxillin.

Supplementary movie 3.

TIR-FSM time-lapse movies of three FA actin binding proteins tagged with GFP: vinculin, talin and α-actinin.

Supplementary movie 4.

TIR-FSM time-lapse movies of GFP-actin and Alexa568-actin. Note that some Alexa568 actin sticks to the coverslip surface during the microinjection procedure.

Supplementary movie 5.

Dual-color TIR-FSM time-lapse imaging of $\alpha_V\beta_3$-integrin-GFP and X-rhodamine-actin and the color coded DCS map.

Supplementary movie 6.

Dual-color TIR-FSM time-lapse imaging of GFP-FAK and Alexa568-actin and the color coded DCS map.

Supplementary movie 7.

Dual-color TIR-FSM time-lapse imaging of GFP-zyxin and X-rhodamine-actin and the color coded DCS map.

Supplementary movie 8.

Dual-color TIR-FSM time-lapse imaging of GFP-paxillin and X-rhodamine-actin and the

color coded DCS map.

Supplementary movie 9.

Dual-color TIR-FSM time-lapse imaging of GFP-vinculin and X-rhodamine-actin and the color coded DCS map.

Supplementary movie 10.

Dual-color TIR-FSM time-lapse imaging of GFP-talin and X-rhodamine-actin and the color coded DCS map.

Supplementary movie 11.

Dual-color TIR-FSM time-lapse imaging of GFP-α-actinin and X-rhodamine-actin and the color coded DCS map.

Supplementary movie 12.

Top row: TIR-FSM time-lapse imaging of GFP-vinculin (green) and X-rhodamine-actin (red) and the color coded DCS map.

Bottom row: color-coded speed map of vinculin (left), F-actin (middle) and the cell-edge trace (right).

Supplementary movie 13. Movies generated by Monte Carlo simulation of fluorescent FA proteins diffusing at the rate shown while bound to an immobile FA platform and uncoupled from a flowing F-actin network (not shown) (diffusion constant D in cm^2/s).

Supplementary movie 14. Movies generated by Monte Carlo simulation to show three levels of coupling (increasing left to right) between fluorescent FA proteins (green) and the F-actin network (red).

Supplementary References:

S1. T. Wittmann, G. M. Bokoch, C. M. Waterman-Storer, *Journal of Cell Biology* 161, 845 (2003).
S2. C. M. Waterman-Storer, *Fluorescent speckle microscopy (FSM) of microtubules and actin in living cells.* . M. D. J.S. Bonifacino, J.B. Harford, J. Lippincott-Schwartz, and K.M. Yamada, Eds. , Ed., Current Protocols in Cell Biology (John Wiley, NY. Unit 4.10. , 2002), pp.
S3. T. E. O'Toole *et al.*, *Blood* 74, 14 (1989).
S4. M. C. Adams *et al.*, *Journal of Microscopy* 216, 138 (2004).
S5. M. Edlund, M. A. Lotano, C. A. Otey, *Cell Motility & the Cytoskeleton* 48, 190 (2001).
S6. S. J. Franco *et al.*, *Nature Cell Biology* 6, 977 (2004).
S7. C. M. Laukaitis, D. J. Webb, K. Donais, A. F. Horwitz, *Journal of Cell Biology* 153, 1427 (2001).
S8. I. Kaverina, O. Krylyshkina, J. V. Small, *Journal of Cell Biology* 146, 1033 (1999).
S9. N. L. Thompson, T. P. Burghardt, D. Axelrod, *Biophysical Journal* 33, 435 (1981).
S10. L. Ji, G. Danuser, *Journal of Microscopy* 220, 150–167 (3 December 2005, 2005).
S11. A. Ponti, P. Vallotton, W. C. Salmon, C. M. Waterman-Storer, G. Danuser, *Biophysical Journal* 84, 3336 (2003).
S12. P. Vallotton, S. L. Gupton, C. M. Waterman-Storer, G. Danuser, *Proceedings of the National Academy of Sciences of the United States of America* 101, 9660 (2004).
S13. A. Ponti, M. Machacek, S. L. Gupton, C. M. Waterman-Storer, G. Danuser, *Science* 305, 1782 (2004).
S14. D. Thomann, D. R. Rines, P. K. Sorger, G. Danuser, *Journal of Microscopy* 208, 49 (2002).
S15. Y. Ohsugi, K. Saito, M. Tamura, M. Kinjo, *Biophysical Journal, in press* (2006).
S16. C. Waterman-Storer, A. Desai, E. D. Salmon, *Methods in Cell Biology* 61, 155 (1999).
S17. W. C. Salmon, M. C. Adams, C. M. Waterman-Storer, *Journal of Cell Biology* 158, 31 (2002).
S18. R. O. Hynes, A. T. Destree, *Cell* 15, 875 (1978).